

The moisture source sequence for the Madden-Julian Oscillation as derived from satellite retrievals of HDO and H₂O

M. Berkelhammer,¹ C. Risi,^{1,2} N. Kurita,³ and D. C. Noone¹

Received 1 September 2011; revised 28 November 2011; accepted 29 November 2011; published 2 February 2012.

[1] A number of competing theories to explain the initiation mechanism, longevity and propagation characteristics of the Madden-Julian Oscillation (MJO) have been developed from observational analysis of the tropical climate and minimal dynamical models. Using the isotopic composition of atmospheric moisture from paired satellite retrievals of H₂O and HDO from the boundary layer and mid troposphere, we identify the different sources of moisture that feed MJO convection during its life cycle. These fluxes are then associated with specific dynamical processes. The HDO/H₂O isotope ratio data show that during the early phase of the MJO, the mid-troposphere is dominated by moisture evaporated from the ocean surface that was transported vertically undergoing minimal distillation. The contribution from the evaporative source diminishes during early convective activity but reappears during the peak of MJO activity along with an isotopically depleted flux, which is hypothesized to originate from easterly convergence. The contribution of different moisture sources as shown from the HDO/H₂O data is consistent with model results where the sustaining of deep convection requires a feedback between convergence, precipitation strength and evaporation. In the wake of an MJO event, the weak vertical isotopic gradient, depletion in boundary layer δD and the uniquely moist and depleted vapor in the mid troposphere all point toward a prominent presence of moisture originated from rainfall re-evaporation, which confirms the prediction that the transition from convective to stratiform rains is important to the moisture budget of the MJO.

Citation: Berkelhammer, M., C. Risi, N. Kurita, and D. C. Noone (2012), The moisture source sequence for the Madden-Julian Oscillation as derived from satellite retrievals of HDO and H₂O, *J. Geophys. Res.*, 117, D03106, doi:10.1029/2011JD016803.

1. Introduction

[2] The Madden-Julian Oscillation (MJO) is the leading source of intraseasonal climate variability in the tropics, whose influence is manifested through its impact on the development of monsoon break cycles [Singh *et al.*, 1992] and tropical cyclogenesis [Camargo *et al.*, 2009]. Its effect on the global climate system can be observed on seasonal to interannual timescales through its modulation of ENSO [Straub *et al.*, 2006] and the state of the North Atlantic Oscillation [Cassou, 2008]. Intensive observational analysis focusing on synoptic circulation and precipitation related to the MJO, depict the system as an envelop of mesoscale convective activity that propagates eastward from the Indian Ocean with a velocity of 4–8 m s⁻¹ [Madden and Julian, 1971; Wheeler and Hendon, 2004; Wheeler and Kiladis,

1999]. Following the seminal description of the system [Madden and Julian, 1972], the MJO is typically broken up into eight “phases” that describe where the center of convection is located along the equator [Madden and Julian, 1972; Wheeler and Hendon, 2004]. Thus, a strong Phase 1 for an MJO is characterized by the presence of a large negative OLR anomaly around 60°E, while Phase 2 of the MJO involves convection centered near 80°E. Each progressive phase marks an increasingly eastward location for the convective center. For a given MJO event, the phases are separated in time by approximately 5–10 days, which equates to an approximate 30–90 day lifespan of the system.

[3] Observational analyses of the MJO characterize the three-dimensional moisture and energy anomalies associated with each phase of the system [Tian *et al.*, 2010, 2006; Jiang *et al.*, 2009; Myers and Waliser, 2003] as well as account for its influence on additional fields such as trace gas variability [Li *et al.*, 2010] and marine productivity [Waliser *et al.*, 2005]. A primary goal of these efforts has been to develop budgets for the MJO to delineate the sources of moisture and energy during the life cycle of an event [Maloney and Hartmann, 1998; Kiladis *et al.*, 2005; Raymond, 2001]. Through careful accounting of energy and moisture, a fundamental theory for the MJO that accounts for its slow

¹Department of Atmospheric and Oceanic Sciences and Cooperative Institute for Research in Environmental Sciences, University of Colorado at Boulder, Boulder, Colorado, USA.

²LMD/IPSL, CNRS, Paris, France.

³Japan Agency for Marine-Earth Science and Technology, Yokosuka, Japan.

propagation speed, geographic preference, unique dispersion characteristics, recurrence frequency and longevity could be developed [Zhang, 2005; Majda and Stechmann, 2009; Majda et al., 2007]. While significant progress has been made in this respect, a unifying theory for the system remains elusive.

[4] Most existing theories of the MJO agree upon some variant of the following sequence where (1) an MJO is initiated by a slow build-up of moisture in the boundary layer over the Indian Ocean [Kemball-Cook and Weare, 2001; Blade and Hartmann, 1993; Majda and Stechmann, 2009], (2) vertical transport of low level moisture through shallow convection acts to pre-condition the atmosphere for deep convection, which after initiation is sustained for multiple days [Benedict and Randall, 2007; Jiang et al., 2009] and (3) trailing to the west of the center of deep convection is a stratiform deck overlain on a dry lower atmosphere [Lin et al., 2004; Tian et al., 2006]. This sequence provides a convenient conceptual depiction for the MJO but the dynamical details pertaining particularly to the initiation mechanism (i.e. internal stochastic vs extratropical forcing) [Ray et al., 2009; Kemball-Cook and Weare, 2001; Hendon and Salby, 1994; Hendon et al., 1998] and moisture cycling are unclear [Zhang, 2005].

[5] The timing of onset and propagation speed for the MJO are thought to be closely tied to moisture-convection feedbacks that influence the transition to and sustenance of the deep convection that is characteristic of the MJO envelope [Grabowski and Moncrieff, 2004; Randall et al., 2003; Majda and Stechmann, 2009; Agudelo et al., 2006]. Insight into these processes has been garnered by attempting to constrain the moisture sources for the MJO using satellite-derived latent heat profiles from the Tropical Rainfall Measuring Mission (TRMM) [Jiang et al., 2009; Masunaga et al., 2006], and three dimensional moisture profiles from the Atmospheric Infrared Sounder (AIRS) [Tian et al., 2006, 2010]. Waliser et al. [2009] generated a moisture budget for the MJO using satellite-derived humidity data and reanalysis products, which suggests that zonal convergence is the dominant moisture source and that surface evaporation plays a more limited role. Both Jones and Weare [1996] and Benedict and Randall [2007] come to a similar conclusion arguing that evaporation anomalies trail convection and therefore could not be priming the atmosphere to the east for deep convection. Seo and Kim [2003] further partition the convergent moisture sources, suggesting one source of moisture is associated with meridional convergence to the immediate east of the convective center while there is a second source further to the east that is responsible for the moist preconditioning of the boundary layer.

[6] These studies are somewhat in contrast to those of Araligidad and Maloney [2008], Maloney and Sobel [2004] and Sobel et al. [2008] who find observational evidence of latent heat flux anomalies of adequate magnitude to sustain the deep convection. A possible reconciliation is offered by Weare [2003] and Kirtman and Vernekar [1993], who suggest that moisture buildup by evaporation occurs in the anomalous dry region well to the east of the active center of the MJO associated with the subsiding limb of the convective circulation. The evaporative flux is reduced in concert with a decrease in the air-sea humidity difference at which point easterly convergence becomes the dominant moisture

source. The disagreement between studies which all attempt to characterize moisture sources for the MJO primarily reflects the fact that the available observational data does not allow for analysis that can clearly delineate moisture sources. Therefore it must be inferred indirectly through budget [e.g., Waliser et al., 2009] or correlation analysis [e.g., Araligidad and Maloney, 2008].

[7] Resolving the uncertainty in the moisture fluxes associated with the MJO can be addressed by modeling studies, where specific processes such as surface fluxes can be traced and/or prescribed [Sobel et al., 2008]. However, because General Circulation Models in general fail to produce coherent MJO events, such diagnostic studies are not currently feasible. The inability of models to produce MJO-like features apparently arises from a lack of necessary convective self-suppression mechanisms, which leads to simulated convective systems that are triggered too quickly and never reach the strength observed during the active phase of the MJO [Slingo et al., 1996; Waliser et al., 1999; MJO Clivar Working Group, 2009; Kim et al., 2009]. Although the MJO representation can be improved in simulations by artificially restraining deep convection until the mixed layer is excessively thick and nearly saturated to its top [Lee et al., 2003; Tokioka et al., 1988], the moisture-convection feedbacks that are necessary for MJO-like variability do not develop intrinsically in models until the vertical and horizontal resolution are substantially increased [Miura et al., 2007] and clouds can be resolved [Grabowski, 2003].

[8] Thayer-Calder and Randall [2009] find that the failure of some models to produce MJOs arises because a close balance between the moisture source (boundary layer air) and sink (precipitation) reduces the ability for models to sufficiently moisten the atmospheric column. The MJO representation is improved when a sequence unfolds where detrainment from low level congestus and light rain initially moistens the atmospheric column [Johnson et al., 1999; Grabowski, 2003; Slingo et al., 1996]. The moistening of the column increases precipitation rates and, as a consequence, there is enhanced surface convergence associated with uplift in the convective region. This precipitation-wind feedback leads to an increase in the availability of moisture from both convergence and surface evaporation. The positive feedback is further sustained because the high humidity throughout the atmospheric column inhibits downdrafts, which would stabilize the column and oppose the moistening from surface air [Emanuel, 1989]. So while both modeling and observational studies have identified potentially critical moist processes for MJO development, neither have been capable of successfully validating the other.

[9] In this study, an analysis is presented of moisture sources associated with the onset and propagation of the MJO using the stable hydrogen isotope ratio in atmospheric water vapor as a tracer for different moisture sources. Joint retrievals of H₂O and HDO from both the Tropospheric Emission Spectrometer (TES) and the Scanning Imaging Absorption Spectrometer for Atmospheric Chartography (SCIAMACHY) are used to derive the isotopic characteristics of the moisture. Heavier isotopologues of water preferentially accumulate in the lower energy state and thus during phases changes there is a temperature-dependent fractionation (i.e. a preferential separation) between water isotopologues [Bigeleisen, 1961]. The rate of diffusion of

heavy isotopes is slower than the common H_2O molecule producing an additional source of fractionation. For example, when moisture evaporates from the ocean surface it must pass through a thin saturated boundary layer. This process takes longer for HDO than H_2O , which results in vapor above the saturated layer having a smaller ratio of HDO to H_2O than the saturated layer below. The distribution of water isotopes in space and time accumulate the influence of these fractionating processes and therefore reflect aspects of the vapor's history including conditions at the source region, the air masses it has mixed with or the extent to which it has experienced rainout. Descriptive and quantitative analyses of isotope ratios in the hydrological cycle have appeared previously and have shown the value of adding isotopic constraints to studies of the atmospheric water cycle [Dansgaard, 1964; Friedman *et al.*, 1964; Craig and Gordon, 1965; Merlivat and Jouzel, 1979; Joussaume *et al.*, 1984; Gat, 2000]. Because moisture phase changes within convective structures (evaporation, condensation) and mixing of air with different isotopic values (i.e. subsidence or convergence) are perceived to be relevant for developing a theory for the MJO, it follows that an isotopic analysis of the system would be beneficial in forwarding a theory for moist processes within the MJO. Specifically, the isotopic analysis sheds light on ocean–atmosphere moisture flux and exchange between hydrometeors and vapor within organized convective systems [Dansgaard, 1964; Lawrence *et al.*, 2004; Risi *et al.*, 2008; Lee and Fung, 2008; Bony *et al.*, 2008; Lee *et al.*, 2009], which have traditionally been challenging to directly observe. The isotopic diagnosis of the MJO presented here therefore attempts to bridge a gap between processes that models predict to be critical for the development and maintenance of MJO events and have yet to be resolved with the existing observational database.

[10] Kurita *et al.* [2011] examined the isotopic composition of water vapor and precipitation during a single weak MJO event and provided the first evidence of the utility of isotopic information as a complement to more traditional methods in diagnosing the hydrology of the MJO. Particularly noteworthy in that study is the identification that boundary layer moisture during the MJO is dominantly influenced by exchange between falling hydrometeors from stratiform precipitation and the underlying atmosphere. The results show that the percentage of stratiform precipitation in the MJO envelop must be accurately represented in climate models in order to reproduce the boundary layer moisture characteristics. The authors also find evidence of the importance of evaporative flux from the marine surface during the build-up phase of the MJO. The findings of Kurita *et al.* [2011] however, leave a number of open questions regarding general characteristics of the isotopic footprint associated with the MJO. For example, because the study was based on a single event, it is not feasible to assess what aspects of the isotopic changes during the MJO are truly systematic. MJO events are characterized by an envelop of small-scale convective systems that vary between events. Therefore, it is unlikely that a single event is generally representative of the system.

[11] The benefit of using isotope ratio data to characterize the atmospheric water cycle is fully realized through spatial and temporal analysis of the joint probability between total water concentration and the isotope ratio of this water.

Consider an air mass whose total water concentration is changing, this observation alone cannot reveal the process driving the moistening or dehydration. However, simultaneous measurements of isotopes can reveal information on the relevant processes acting to change the hydrology [Webster and Heymsfield, 2003; Galewsky *et al.*, 2007; D. Noone *et al.*, Pairing measurements of the water vapor isotope ratio with humidity to deduce atmospheric moistening an dehydration in the tropical mid-troposphere, submitted to *Journal of Climate*, 2012]. The classical example of how this manifests is through the equation that describes Rayleigh distillation, where the immediate loss of moisture through condensation produces a reduction in the ratio between the heavy and common water isotopologues and moisture that falls along a predictable trajectory in the water-isotope space [Friedman *et al.*, 1964; Jouzel, 1986; Noone, 2012]. Deviations from this trajectory reveal processes acting on the vapor such as mixing from an additional moisture source or precipitation efficiency that is less than 1 [Worden *et al.*, 2007]. Therefore a series of simple models derived from the Rayleigh distillation equation and end-member mixing models can be applied toward understanding information on the history of water vapor at a given location in space and time (Noone *et al.*, submitted manuscript, 2012). Within the framework of these simple models that describe joint changes in water and δD , a water budget for the MJO is developed. While similar information can be derived through classical meteorological fields by way of trajectory analysis and careful budgeting of fluxes, these techniques do not provide direct measures of the characteristic history of a vapor mass.

[12] In the first part of this paper a series of diagnostic analyses are used to clearly identify the space and time variations in water isotopes associated with the MJO. In the second part of the study, a water budget analysis highlights major transitions of the MJO moisture sources during initiation, onset of deep convection, the passing of the stratiform ledge and ultimately in the wake of the system. The study concludes with a discussion on how these observations are useful in resolving a number of competing theoretical depictions of the MJO, namely in clearly identifying the relative significance of evaporation and convergence in providing moisture to sustain convection. The results presented have immediate implications with respect to validation of these theoretical depictions of the MJO water budget and also may yield a more direct practical application in light of the observation that the isotopic composition of vapor during early initiation of the MJO may serve as a good predictor of MJO development.

2. Methods: Data Sets

[13] The primary data set employed in this study is the Version 4 and 5 retrievals of HDO and H_2O from TES, which is a high-resolution infrared spectrometer aboard NASA's AURA spacecraft. The retrievals provide global coverage of atmospheric δD profiles with maximum sensitivity between the 850–500 hPa level [Worden *et al.*, 2006]. Retrievals from the 600 hpa level from July 2005 through December 2009 were used. In the tropical latitudes, the error on HDO measurements is less than 10% resulting in a δD error of less than 10‰ [Worden *et al.*, 2007]. All data were subjected to quality control following the work of

Worden *et al.* [2006] and Worden *et al.* [2007], which includes correction of a documented bias associated with the HDO estimates [Worden *et al.*, 2010] and an additional requirement that all measurements must have a degree of freedom from the a priori that exceeds 0.5 [Brown *et al.*, 2008; Lee *et al.*, 2011]. Filtering the data tends to remove measurements taken during periods of high cloud optical depth and thus subsequent analysis is weighted toward vapor existing in the region surrounding the deep clouds [Lee *et al.*, 2011]. Lee *et al.* [2011] find that the retrievals of HDO from TES infrared spectra are sensitive to cloud type, however this sensitivity produces only a modest artifact ($\sim 5\text{--}10\%$) on the comparison of isotope ratio values from different cloud domains. Analysis of composites minimizes the influence of this bias in the results. The findings are based on features that are of a magnitude, which exceeds the uncertainty associated with both the measurement and the cloud sampling bias.

[14] A specific quantification of instrument sensitivity for the domain and time period of the data in this study is estimated by collocating all TES retrievals that pass the quality criteria described above with outputs from an isotope-enabled general circulation model (LMDZiso) [Risi *et al.*, 2010]. A comparison between raw model isotopic outputs and those convolved by the averaging kernels used for the TES retrievals [i.e., Worden *et al.*, 2006] yields an estimate on the extent to which the instrument sensitivity influences the absolute value and variability of the satellite-derived isotopic ratios. The results of this calculation suggest that the highest δD values ($\geq -120\%$) are systematically underestimated by 5% while the lowest values ($\leq -200\%$) are systematically overestimated 25%. Therefore, the instrument sensitivity of TES reduces the isotopic range by about 25–30%. Thus, the results presented throughout this study likely represent a conservative representation of the actual isotopic variations.

[15] The δD is calculated in ‰ units by dividing the molar ratio of HDO to H₂O from that of Vienna Standard Mean Ocean Water, subtracting unity and multiplying by 1000 (see equation (6)). Where possible, all analyses were based on corrected satellite estimates that have not been subjected to any interpolation. However, to accommodate spectral analysis and the requirement for continuous spatial and temporal fields, δD was binned onto a 3.75° longitude by 2.5° latitude global grid and five-day (pentad) averages were calculated. In instances where no data was present after binning and pentad-averaging, the Poisson grid-filling algorithm from the NCAR Command Line package was used to produce a continuous spatial and temporal isotopic field.

[16] Estimates of the HDO/H₂O ratio of lower atmospheric δD were taken from the Scanning Imaging Absorption Spectrometer for Atmospheric Chartography (SCIAMACHY) aboard ESA's environmental research satellite [Frankenberg *et al.*, 2009]. The dataset has previously been validated through comparison with in situ observational measurements of δD . As opposed to TES, this data yields column-integrated HDO and H₂O, which provide an estimate of δD that is heavily-weighted toward the lower 2 km of the atmosphere. As a consequence, SCIAMACHY retrievals have significantly higher ratios of HDO/H₂O, which reflects the isotopic composition of boundary layer air, which is strongly

influenced by surface fluxes that are depleted by the time they reach the mid-troposphere (i.e. where TES retrievals are most sensitive). The retrievals were filtered to remove instances where the column integrated water concentration differed by greater than 10% from that estimated from the ERA-40 Reanalysis model [Uppala *et al.*, 2005]. Because of the uncertainty on individual measurements (40–100%) and a very limited number of reliable measurements over the ocean, analysis is only performed after the data has been averaged over large spatial (10° × 10°) and temporal (10-day) domains. The difference in overlapping regional averages between TES and SCIAMACHY is used to provide an estimate of the “isotopic lapse rate”, which varies in response to vertical mixing, precipitation efficiency and exchange processes [Rozanski and Sonntag, 1982; Ehhalt *et al.*, 2005].

[17] Additional meteorological fields from Global Modeling and Assimilation Office-Modern Era Retrospective-Analysis for Research and Applications (GMAO-MERRA) Reanalysis model (temperature, rainfall evaporation, moisture convergence, latent heat flux, vertical velocity, specific humidity and cloud type/cover) [Rienecker *et al.*, 2011], the Global Precipitation Climatology Project (rainfall) [Adler *et al.*, 2003], NCEP-DOE Reanalysis II (wind fields, latent heat flux and specific humidity) [Kanamitsu *et al.*, 2002] and the NOAA daily interpolated Outgoing Longwave Radiation (OLR) product [Liebmann and Smith, 1996] are used to understand processes influencing the isotopic composition of the water vapor. Identical analyses are performed for GMAO-MERRA and Reanalysis II in order to minimize the likelihood that conclusions are based on a bias in a single reanalysis model. This is particularly necessary for surface heat fluxes and cloud properties, which are diagnostic products from the Reanalysis and so less robust. While climate models in general fail to produce MJO events, the Reanalysis models are constrained by satellite, ground-based and radiosonde observations, which results in reasonable representation of the large scale features of the MJO [Kim *et al.*, 2009].

3. Methods: Analytical

[18] To assess the strength of the MJO signature on atmospheric δD , a suite of MJO diagnostics following the recommendations of Waliser *et al.* [2009] and Wheeler and Hendon [2004] are used. δD anomaly maps for each of the eight phases of the MJO are calculated by projecting isotopic anomalies onto an MJO index derived from a multivariate empirical orthogonal function analysis of OLR, 200, and 850 hPa wind fields. To quantitatively diagnose the MJO signal in the isotopic field, space-time spectral analysis is performed, which isolates isotopic variability with the unique wave dispersion characteristics, slow propagation speed and geographic preference of the MJO [Wheeler and Kiladis, 1999]. The space-time spectra for δD is calculated using a multitaper approach and significance is estimated relative to a reddened background spectra which is calculated by progressively smoothing the spectra using a 1-2-1 filter until all non-random signals are removed [Kiladis *et al.*, 2009]. The calculated spectra is subtracted from the background and all values exceeding the 95% confidence interval are retained. Characteristic wave types are

distinguished using solutions for wave dispersion derived from the shallow water equations [Matsuno, 1966; Kiladis *et al.*, 2009].

[19] In order to isolate the climatic processes that influence the isotopic composition of the moisture, the phase angle between isotopic variability and relevant climate processes (e.g. wind, moisture convergence, precipitation) is calculated. For this analysis, an areally-averaged δD time series is produced for 2005–2008 from the core of the MJO domain (80–120°E and 12°S–12°N) and an assumption is made that variability with 30–90 day periodicity arises principally from the MJO. Cross-spectral analysis between the δD time series and meteorological fields indicative of MJO activity such as OLR, specific humidity and rainfall are calculated using a multitaper method [Chave *et al.*, 1987]. The coherence and phase are then used to estimate whether the given process influences the isotopic signature associated with the MJO and at which point in the MJO life cycle this process is significant. Uncertainty in the estimate of phase is calculated using a Monte-Carlo procedure where numerous (500) random time series with similar spectral features as the δD time series and the relevant climate field are generated. For each of these randomly generated time series, cross spectral analysis is performed which results in a distribution of possible phase angles that could arise purely from chance given time series with these same spectral characteristics. The phase angle between δD and each field is then presented as a distribution based on the results from the Monte Carlo simulation.

3.1. Moisture Source Isotope Ratios

[20] One approach toward isolating the moisture sources influencing an air mass is to explicitly solve for the isotopic composition of the flux term using a budget equation. By resolving the isotopic composition of the flux, some constraints can be placed on the moisture feeding the system. For example, moisture evaporated from the tropical ocean has an isotopic composition of $\sim -80\%$. A simple budget equation for moisture in an air mass must account for vapor that preexists, vapor that is added by a convergent flux and moisture that is lost by a sink (condensation). The isotopic ratio is thus governed by:

$$\frac{dq \times \delta D}{dt} = F \times \delta D_{flux} - C \times \delta D_{sink} \quad (1)$$

where F is the flux and C is the condensation sink. Because δD is not a conservative quantity, the equation must be rewritten as a budget for both HDO and H₂O separately and the isotopic composition of the flux is then estimated from the results of the two isotopologue budgets. For the water vapor mixing ratio, q , the budget equation is:

$$q_t = q_{t-1} + dt \times (q_{flux} - q_{condensation}) \quad (2)$$

[21] The concentration of water is taken directly from the TES retrievals, and condensation amount is taken from the MERRA reanalysis archives where cumulative (large scale + convective) precipitation production (archived in units of $\text{kg kg}^{-1} \text{day}^{-1}$) integrated between the 600–700 hpa level is used. An analogous equation for HDO is written as

follows, where HDO concentrations are taken directly from the TES retrievals:

$$\text{HDO}_t = \text{HDO}_{t-1} + dt \times (\text{HDO}_{flux} - \text{HDO}_{condensation}) \quad (3)$$

[22] Because the HDO concentration in the condensate is unknown, an assumption is made that the precipitation forms in isotopic equilibrium with the vapor and the ratio of HDO to H₂O in the condensate can thus be estimated with the following equation:

$$\delta D_{condensation} = \delta D_{vapor} + (\alpha - 1) \quad (4)$$

and α is given by Majoube [1971]:

$$\ln \alpha_{HDO} = \frac{24844}{T^2} - \frac{76.248}{T} - 0.52612 \quad (5)$$

where T is temperature in kelvins, which was taken from the MERRA archives. For each daily time step, the flux of HDO and H₂O is thus calculated separately and the resulting terms are converted to δ -notation using the following equation:

$$\delta D_{flux} = \frac{\frac{\text{HDO}_{flux}}{q_{flux}}}{\frac{\text{HDO}_{oceanwater}}{q_{oceanwater}}} - 1 * 1000 \quad (6)$$

[23] A band pass filtered (Lanczos filter, low-pass 30 days) time series of H₂O is used to identify sustained periods where the atmosphere is primarily being moistened (i.e. $d(\text{H}_2\text{O})/dt > 0$) and the isotopic composition of the moisture flux derived from equations (1)–(6) is calculated over the region bounded by 80–120°E and 12°S–12°N for each day during these sustained intraseasonal moistening periods (i.e. the MJO). The daily flux estimates are then separated into the moisture flux associated with the first half of the moistening sequence and the flux associated with the second half of the moistening period. Splitting the sequence in half represents an arbitrary break point, which is used to test whether the moisture flux changes during the evolution of the system. Hereafter, the early half is referred to as “Onset/Initiation” and the second half as “Peak”. This same procedure is repeated for both the western Indian Ocean (80–120°E and 12°S–12°N) and for a region in the tropical/sub-tropical N. Atlantic Ocean (35–55°W and 12°N–22°N). These regions were selected to address whether the evolution of moisture flux for the MJO is simply characteristic of all large-scale convective activity or whether its evolution, with respect to moistening processes, differs fundamentally. The regions selected both exhibit significant intraseasonal variability on timescales that are comparable to the MJO, which makes them suitable for this type of comparison.

3.2. Composite Analysis of MJO Events

[24] Traditional MJO diagnostic analyses characterize the strength of an MJO based on deviations in wind and OLR in subsequent eastward domains of the Indian Ocean and Tropical Pacific [Wheeler and Hendon, 2004]. It is the sustained eastward propagation at speeds of 4–8 m s^{-1} that distinguishes the MJO from other strong convective systems in the Indian Ocean. Using these established diagnostics, ten MJO events were selected from the period between 2005–

Table 1. List of MJO Events Used to Generate the Isotope Composites

Event Duration	Satellite	RMM1 ² + RMM2 ^{2a}	EEOF/CPC
8/26/05–9/25/05	TES	3.9	1.7
10/30/05–11/24/05	TES	4.3	1.5
6/17/06–7/12/06	TES	1.3	1.0
12/19/06–1/13/07	TES	4.9	1.8
2/17/07–3/9/07	TES	3.7	1.4
6/7/07–7/22/07	TES	1.5	1.3
12/9/07–1/18/08	TES	4.1	1.6
3/9/08–4/8/08	TES	1.0	1.4
4/3/09–5/8/09	TES	4.7	1.7
11/4/09–11/29/09	TES	3.4	1.8
12/4/03–1/18/04	SCIAM	4.4	1.5
1/23/04–2/22/04	SCIAM	3.7	1.6
3/9/04–3/29/04	SCIAM	6.3	1.0
4/28/04–5/18/04	SCIAM	3.4	1.5
6/2/04–7/7/04	SCIAM	2.5	0.8
9/20/04–10/20/04	SCIAM	2.3	0.9
12/29/04–1/23/05	SCIAM	2.1	1.3
3/24/05–4/28/05	SCIAM	7.7	1.5
5/3/05–5/23/05	SCIAM	5.2	1.6
8/26/05–9/25/05	SCIAM	2.8	1.3

^aWheeler and Hendon [2004].

2009 where the amplitude of the event remains near to one standard deviation greater than the mean normalized value for each consecutive 8 phases of the MJO. The events chosen represent approximately the strongest 50% of the MJO events during this period. Because subtle differences exist in the approach of characterizing the strength of an MJO event, those chosen for the composite isotopic analysis were required to pass the threshold criteria on both the multivariate MJO index of Wheeler and Hendon [2004] and one based on an extended empirical orthogonal function analysis of the 200 hPa wind fields (cpc.ncep.noaa.gov/products/precip/CWlink/daily_mjo_index/proj_norm_order.ascii) (Table 1).

[25] For each of the selected MJO events, the joint probability density function of H₂O and δ D for a fixed region in which convection associated with the MJO dominates (90–120°E and 12°S–12°N) is calculated for progressive pentads as the system develops and dissipates in this region. The approach deviates from traditional MJO analysis in that it does not follow the event eastward but rather characterize its buildup and dissipation from a fixed location. The analysis focuses on four consecutive pentads prior to the peak of the MJO (centered at –17.5, –12.5, –7.5 and –2.5 days) and continues for four pentads after the MJO has reached its peak (centered at +2.5, +7.5, +12.5, +17.5). The joint density of H₂O and δ D is calculated for each pentad using a non-parametric kernel density estimation approach for each of the ten events and the resulting probability density functions (PDFs) are averaged together as an arithmetic mean and subtracted from the cumulative PDF for this region calculated from all available retrievals. The calculation of the bivariate PDF follows the methods of Botev *et al.* [2010] where a Gaussian kernel is used and the bandwidth is optimized. This procedure produces a bivariate PDF anomaly map for each stage of the MJO that highlights how the moisture characteristics evolve. In order to interpret the cause of the moisture anomalies in the PDFs, the anomaly maps are compared against the isotopic process models from Noone *et al.* (submitted manuscript, 2012), which were parameterized using known values for kinetic

and equilibrium isotopic fractionation [Merlivat and Jouzel, 1979; Stewart, 1975; Jouzel, 1986] and initialized using an average value for moisture evaporating from the warm tropical ocean (δ D = –80‰).

[26] With respect to moisture sources for the MJO, the isotopic information proves most useful through generating phase diagrams that trace the trajectory of δ D–H₂O pairs through the life cycle of the system. The phase diagrams were calculated from the same composite data set used to generate the PDF anomaly maps except that for each progressive pentad, the expected δ D and H₂O is calculated as well as the extrema of the joint-PDF, which leads to a scalar representation (as opposed to distribution) of the characteristic vapor during an MJO life cycle. An identical analysis was performed for a region in the Atlantic (described above), to determine whether the isotopic-phase of the MJO is unique or simply characteristic of all sustained organized convection. Lastly, phase diagrams were also produced for the boundary layer moisture using isotopic retrievals from the SCIAMACHY data set. The δ D and H₂O from TES and SCIAMACHY for each phase are subtracted from one another to identify secular trends in the “isotopic lapse rate”. The vertical profile of the isotopic composition of vapor is important for distinguishing vertical mixing or detrainment of boundary layer water by shallow clouds. For example, the characteristically steep isotopic gradient associated with pure Rayleigh distillation (i.e. preferential rainout of HDO to H₂O with height) is relaxed when vertical mixing brings vapor with relatively high isotope ratios to altitude [Webster and Heymsfield, 2003] or when depleted moisture from height is mixed downward [Bony *et al.*, 2008].

[27] Uncertainty on the estimate of mean values is expressed throughout the paper using standard error, $\frac{s}{\sqrt{n}}$, where s is the standard deviation and n is the total number of retrievals that compose the mean value.

4. Results

4.1. Spatial and Spectral Isotopic Footprint of the MJO

[28] In Figure 1, composite δ D anomaly maps are shown for each of the eight phases of the MJO [Wheeler and Hendon, 2004]. The results suggest the MJO is associated with an eastward propagating couplet of moisture with high and low isotope ratios. In the developing stages (Index 1 and 2), the amplitude of the positive anomaly is small (5–10‰) but grows progressively (16–20‰) as the system propagates to the dateline. While the sensitivity of individual δ D retrievals from TES is 10‰, because the composites are developed from a large number of retrievals, the main spatial structure for each of the phases is robust while individual data may not be (standard error maps for each phase are shown in auxiliary material Figure S1).¹

[29] A Hovmöller plot of a section of the data produced from band-passed (30–90 days) δ D and OLR anomalies is shown in Figure 2. Long-lived and slowly propagating isotopic anomalies are recurrent west of the dateline and are often parallel or synchronous with OLR anomalies. A few examples of these systems are highlighted by white dotted

¹Auxiliary materials are available in the HTML. doi:10.1029/2011JD016803.

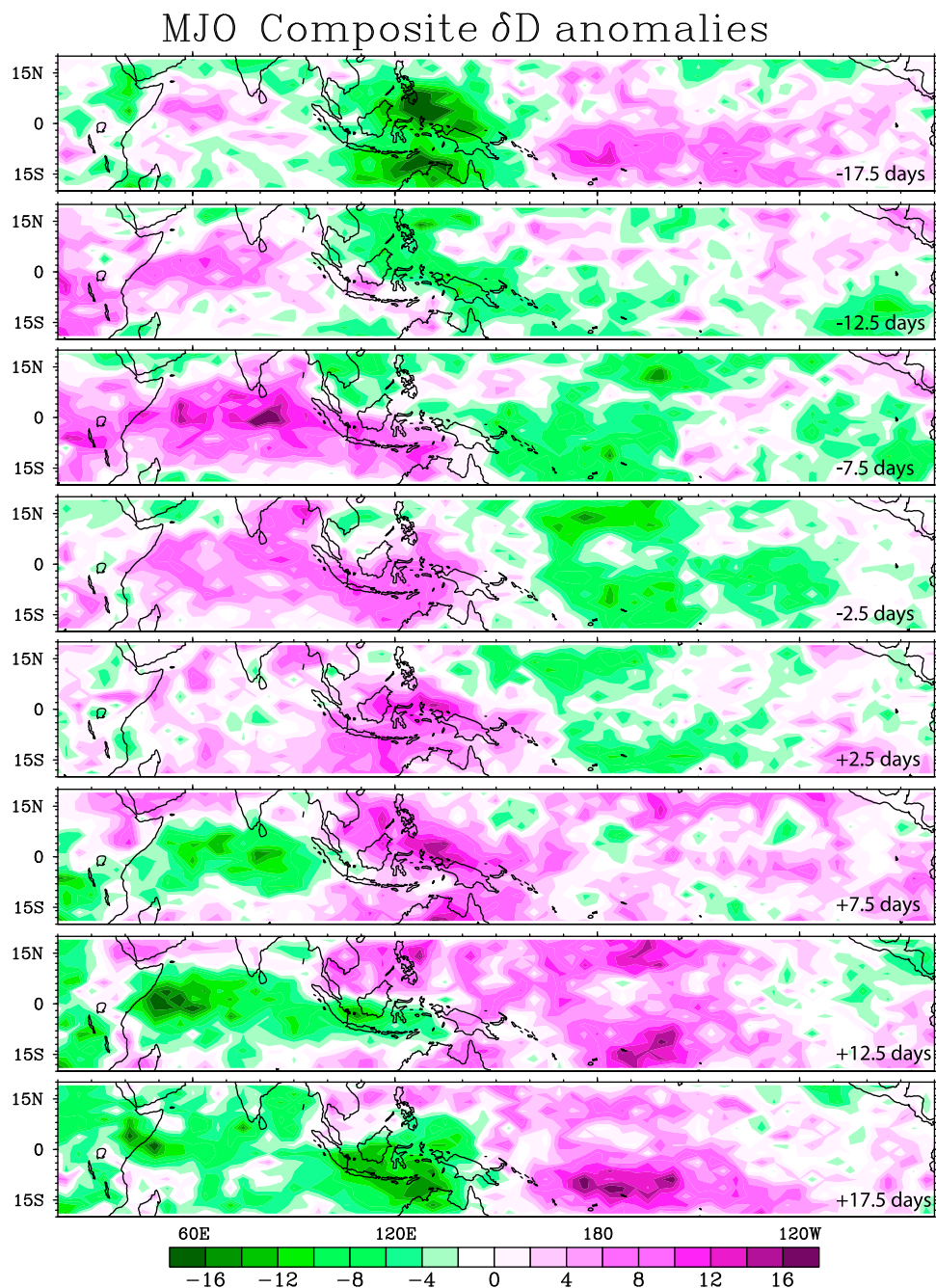


Figure 1. Composite map of the δD anomalies for progressive phases of the MJO. The figure was created using a multivariate EOF analysis of OLR, 200 hPa U-winds and 850 hPa U-winds from NCEP Reanalysis and projecting isotopic anomalies on the MJO index derived from the leading two principal components of the EOF analysis.

lines in Figure 2. We also note high amplitude isotopic signals in the eastern Tropical Pacific though these appear as faster moving and shorter-lived systems. While these features are not diagnosed explicitly here, it is hypothesized that they likely arise from the sensitivity of TES δD to large-scale subsidence in the descent region of the Walker circulation as this process involves the mixing of dry, isotopically depleted air into the mid-troposphere.

[30] The results from the space-time spectral analysis of δD show a pronounced MJO signal, characterized by

eastward propagating waves, with periods of 30–90 days and wave numbers between 1 and 2 [e.g., *Wheeler and Kiladis, 1999*] (Figure 3). There is significant power also associated with westward propagating Rossby waves (i.e. the eastern Tropical Pacific features from Figure 2) and a higher wave number signal, which arises from the 16-day recurrence frequency of identical passes by Aura. Space-time spectral analysis is conducted for the TES H_2O field, which reveals the presence of both an MJO signal and one associated with westward propagating Rossby waves. The most prominent

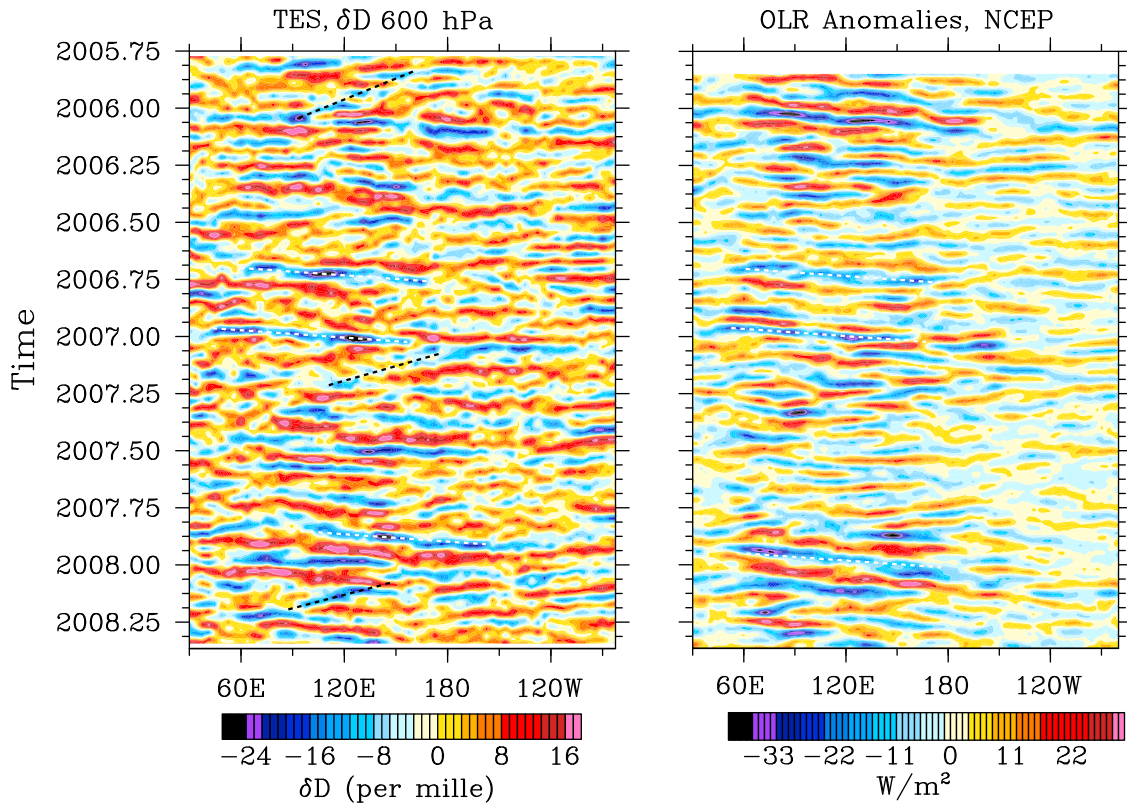


Figure 2. (left) Hovmöller plot of band-pass (30–90 days) filtered δD anomalies and OLR anomalies. The data was filtered with a Lanczos filter using all values falling between 15°S to 15°N latitude. (right) The same analysis was done with the NOAA OLR daily interpolated data set. White dotted lines are used to emphasize pronounced MJO events in the isotopic and OLR fields and black dotted lines indicate Rossby waves with depleted isotopic ratios.

difference between the water and isotopic fields is the presence of a Kelvin wave signature in water that is not apparent in the δD field. The absence of this signature in δD may arise as a product of data quality issues, where missing data points would remove or obscure certain higher frequency cycles. An alternative physical explanation of this observation is

that, unlike Rossby waves, Kelvin waves are not associated with material transport, and therefore the history of the vapor in an air mass is not propagated downstream.

[31] Similar space-time spectral analysis of other meteorological fields are calculated in order to confirm the lack of Kelvin wave signature in δD is associated with material

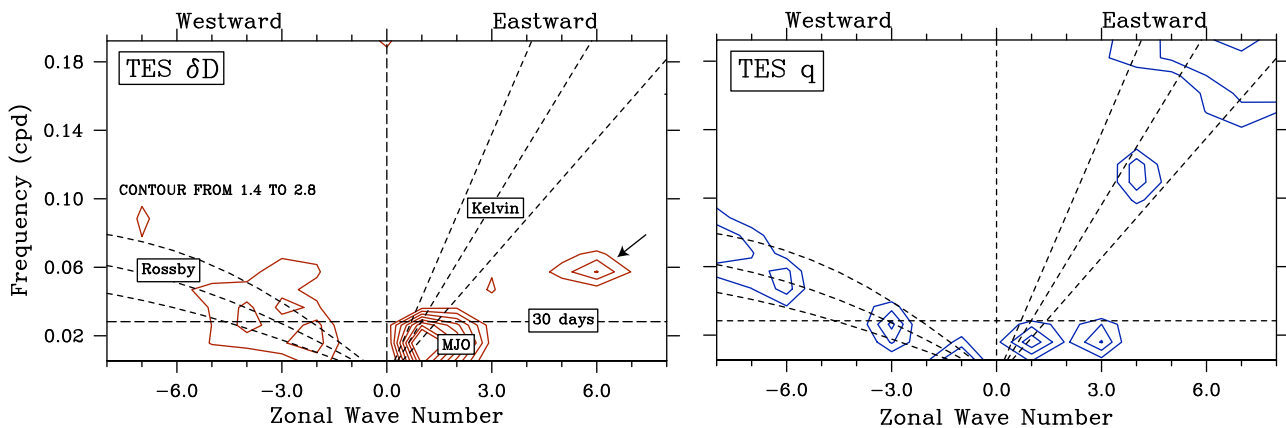


Figure 3. Time-space spectral analysis for (left) δD and (right) H_2O mixing ratio, q . Dispersion curves for equatorial Rossby and Kelvin waves are shown as dotted lines [Wheeler and Kiladis, 1999]. Only contours that are significant ($\geq 95\%$) above a red noise background are plotted in units of log-power in 0.2 contours. The arrow marks the signal associated with the AURA recurrence frequency.

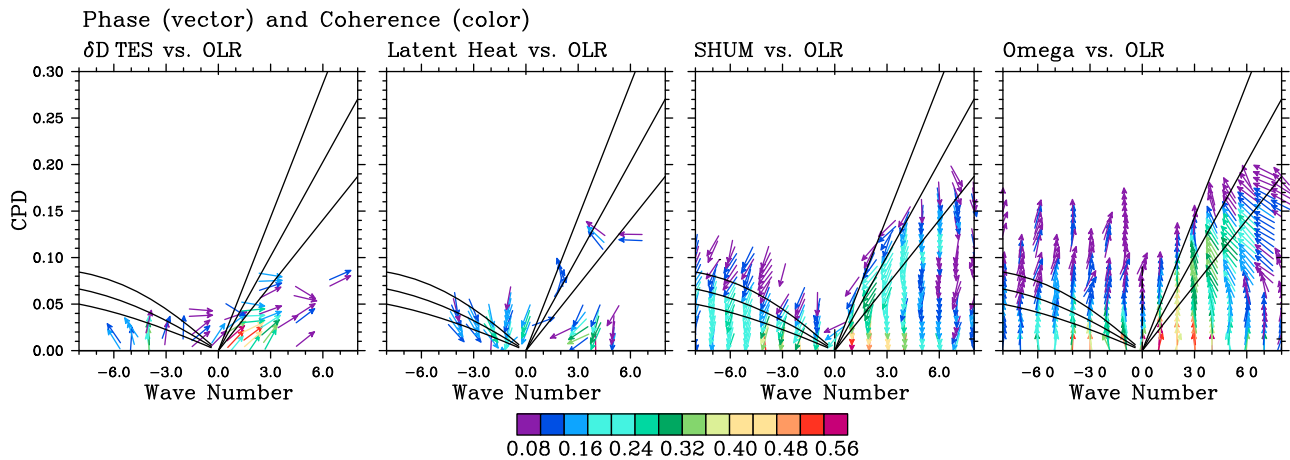


Figure 4. Time-space cross spectral analysis for different fields against OLR. Vectors show the phase (in-phase horizontal right) for all points where the coherence between variables is significant. Colors are used to denote the strength of the coherence. The dispersion curves are identical to those shown in Figure 2.

transport (Figure 4). It is shown (as discussed by *Wheeler and Kiladis* [1999]) that pronounced MJO and Kelvin wave signals are seen in OLR, integrated specific humidity and vertical velocity (ω). However, similar to δD , surface latent heat flux is insensitive to Kelvin waves. The absence of a Kelvin wave signature in latent heat flux may also explain the lack of a similar signal in the δD field as the ratio of H_2O/H_2O is particularly sensitive to moisture flux from surface evaporation. Although the latent heat flux field is a diagnostic product from the Reanalysis model and therefore sensitive to how surface fluxes are represented, large-scale changes in this field are ultimately sensitive to meteorological drivers, which are robust in the Reanalysis model.

4.2. Phase Relationship Between δD and Other Meteorological Parameters

[32] Using a single MJO event as a case study, *Kurita et al.* [2012] identify a significant transition in the δD of vapor during the MJO associated with the transition between relatively enriched moisture from evaporative flux and vapor that has been depleted by post-condensational exchange as the prevalence of stratiform rain in the MJO envelop increases. In Figure 5, an extension of this analysis is presented by considering the phase relationship between the satellite-derived δD for all MJO events during the 2005–2009 time period and a number of Reanalysis fields. The maximum value for δD occurs at the point in time denoted by the dotted line (i.e. Day 00) in Figure 5. Thus, the relationship between the isotopic composition of the moisture and the meteorological fields are presented with respect to the peak in δD . As indicated from the autocorrelation function of δD (Figure 6), the minima in δD occurs approximately 20–30 days after this peak. Therefore, those meteorological fields that have a maximum lag in the 20–30 day window are roughly in anti-phase with δD while those that cluster near Day 00 exhibit an in-phase relationship. Other aspects of the phasing relationships between non-isotopic meteorological data are also implied from this analysis such as the anti-phased behavior between OLR and ω .

[33] Prior to the peak in δD , there is an intraseasonal peak in ω , which is associated with a suppression of cloud formation. This is followed by maxima in meridional surface winds (denoted “Merid.”) and surface evaporation (Evap.), which both increase nearly synchronously with δD but reach their peak values slightly after δD . As δD begins to drop (i.e. following Day 00, Figure 5), there is a rise in integrated positive zonal moisture convergence (denoted “H₂O conv.”), which has a vertical maximum in this region at the 850 hPa level. This is followed by peaks in 850 and 650 hPa specific humidity (SHUM), the latter of which is calculated using both Reanalysis data and from TES H₂O. Between 15–20 days after the δD maximum, precipitation (Precip.) and negative OLR anomalies (indicative of the peak in MJO activity) reach their maxima. 2–4 days after the peak in MJO activity, the maxima in stratiform cloud cover (H. Cld.) and rainfall evaporation (Rain Evap.) occur.

[34] The phase calculations depict a sequence where drying of the boundary layer promotes evaporation, which results in a rise of isotopic values. In general the flux from surface evaporation will be enriched relative to the background moisture as a consequence of the moisture having yet to undergo any distillation. The specific isotopic ratio of the evaporating moisture will vary as a consequence of sea surface temperature and the thickness and stability of the boundary layer between the ocean and atmosphere, which influences the extent to which diffusion will deplete the flux in heavy isotopes. During strong surface winds, the conditions will be primarily turbulent and thus little fractionation by diffusion will occur [*Craig and Gordon*, 1965]. Furthermore, in stormy conditions sea spray may significantly enhance the isotopic ratio in the air as this will produce a moisture source that is identical to that of the ocean [*Lawrence et al.*, 2004]. As evaporation declines, zonal convergence becomes more prominent and the isotopic values experience a progressive decline. It is not clear from the phase analysis alone whether the increase in easterly convergence has a direct causal influence on the decline in δD or whether the statistical relationship reflects the

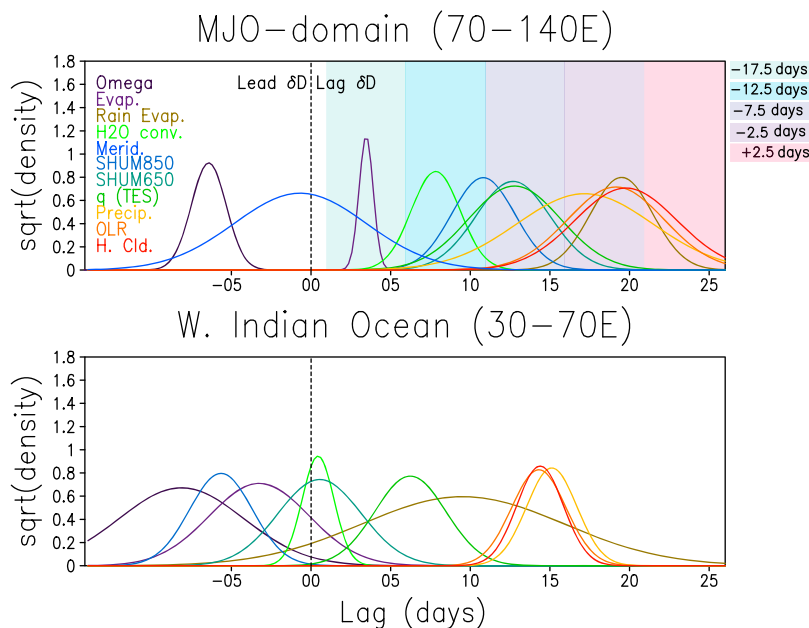


Figure 5. Phasing relationships in the 30–90 day window between δD and a series of climatological fields that are considered influential on the initiation and/or maintenance of the MJO. The phasing was calculated using a multitaper coherence estimate [Chave *et al.*, 1987]. Probable phasing is plotted as gaussian distributions based on the results from a Monte Carlo simulation (see text for details). Fields that plot to the left of the dotted line are those that lead the maxima in δD (as indicated by the dotted line) while those to the right, lag the maxima in δD . The minima in δD occurs at approximately the 25-day mark and therefore the fields that fall in this region are in near-antiphase with δD . The $\sqrt{\text{density}}$ is used as the unit for cosmetic reasons (i.e. to reduce the spread of values on the y axis). (top) The analysis was done for the MJO region and the progressive colored bars track the maturity of the system and delineate the pentad time steps used in Figures 7 and 8 (i.e. Days relative to the peak of MJO based on OLR). (bottom) The same analysis but done for the region to the immediate west of the MJO domain.

increasing presence of stratiform rains and associated post-condensational exchange during the maturity of the MJO envelope [Kurita *et al.*, 2012]. Using ground-based radars, Yamada *et al.* [2010] note that during the development of Super Cloud Clusters [Nakazawa, 1988] associated with the MJO, strong easterly convergence in the mid-troposphere can have zonal distances on the order of a few degrees. It could be inferred from these observations and those presented in Figure 5 that there is an increase in the presence of regional moisture relative to the local evaporative flux during the buildup of the MJO. This moisture would be depleted with respect to the local source if it had experienced any previous condensation. Figure 2 suggests that in some instances during initiation of an MJO event, westward propagating Rossby Waves may be responsible for the convergence of moisture with relatively low isotopic ratios. The importance of Rossby waves in triggering MJO events is well-documented elsewhere [Matthews, 2000], however, their direct role in long distance moisture transport has yet to be explicitly documented.

[35] Throughout the MJO sequence, the atmospheric column is moistening from the bottom up and as precipitation increases in step with the moistening atmosphere, the isotopic values continue to decline, reaching their minimum value at the peak of stratiform rainfall. The decline of the isotope ratios during the increase in MJO activity is consistent with the inverse relationship between precipitation

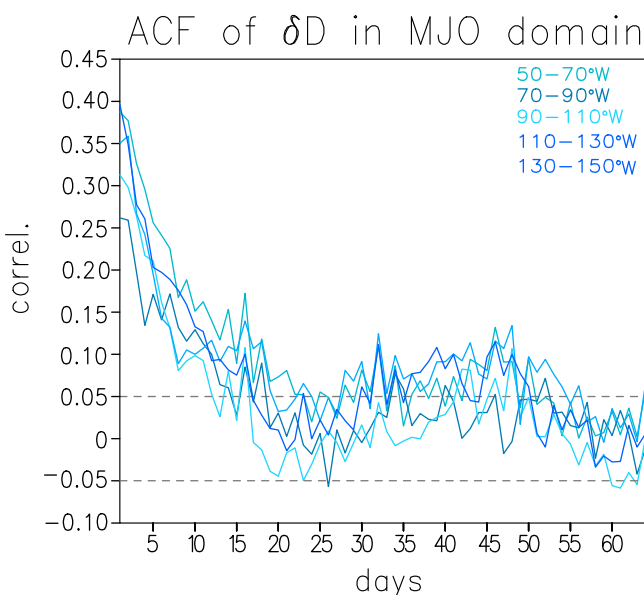


Figure 6. A series of autocorrelation functions for TES δD values for boxes encompassing the MJO domain. All boxes extend from 12°S to 12°N latitude. The dotted line represents correlation coefficients that are significant at $p < 0.05$ relative to a white noise alternative.

Water Content of MJO

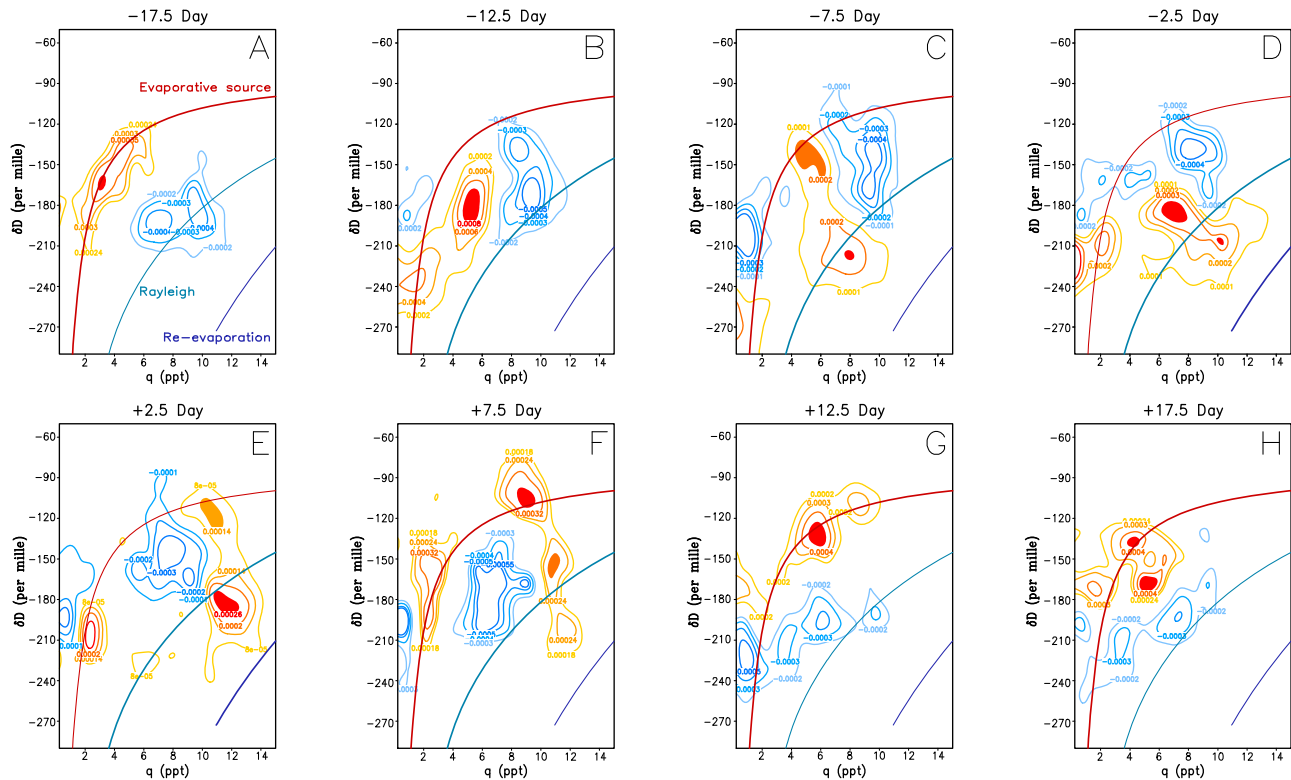


Figure 7. The bivariate probability density function of δD and water observed from TES in the region bounded by 12°S to 12°N latitude and 90° – 120° longitude at 5-day time increments prior and after a passing MJO event. At each time interval a composite PDF for all events listed in Table 1 was created using an adaptive kernel density procedure following *Botev et al.* [2010] and this value was subtracted from a background PDF (see auxiliary material Figure 1) generated using all observations from said region. Therefore, positive values (red) represent moisture that is anomalous relative to the mean for this region. The filled contour regions identify the extrema of each map and are the values used to generate the phase diagrams in Figures 8a and 8b. The lines, which are labeled only in the first panel, are theoretical trajectories for moisture that is undergoing mixing (red), condensation (blue) or condensation recycling (purple) processes. The derivations for the equations for these models are presented by Noone et al. (submitted manuscript, 2012) and described in the text.

amount and isotope ratios (i.e. the “Amount Effect”) as has been directly observed [*Dansgaard, 1964; Kurita et al., 2009*] and diagnosed in model simulations [*Risi et al., 2008; Lee and Fung, 2008*]. Using a model simulation that has been nudged to meteorological fields and fitted with isotopic tracers, *Kurita et al.* [2012] find that during the peak of simulated MJO events, the primary mechanism that leads to the depletion in isotopic values is post-condensational exchange that occurs as stratiform rains formed high in the troposphere fall through the atmosphere. This was also noted in the work of *Lawrence et al.* [2004], which showed that in long-lived convective systems these exchange processes are necessary to explain the observed low δ values in precipitation. The phase relationship also suggests that the isotopic depletion in the MJO moisture arises as a consequence of rainfall evaporation, which is associated both with large-scale subsidence and unsaturated downdrafts, which transport air containing vapor with low δD from higher altitudes in the mid-troposphere downward [*Risi et al., 2008*].

[36] A similar phase analysis is conducted for the oceanic region to the west of the MJO domain (western Indian Ocean, hereafter WIO). The results are used for comparative purposes as this region experiences organized convective systems that do not propagate or persist like the convection associated with the MJO (Figure 5). In the WIO, the sequence shares some clear similarities to that which occurs in the MJO domain (drying-evaporation-convergence-precipitation) but unfolds over a shorter period of time (12–16 days). One noteworthy difference between the two is that intraseasonal δD variability in the WIO is disconnected from rainfall evaporation as inferred from the very large uncertainty in the phase angle associated with this variable. Recall that in the MJO domain, rainfall evaporation appears tightly connected with δD , reaching its peak during the δD minima. To the extent that rainfall evaporation is closely tied to stratiform precipitation, the difference in the two domains with respect to this variable, may reflect a causal need for large-scale stratiform precipitation to sustain the MJO [*Lin et al., 2004*]. The other notable

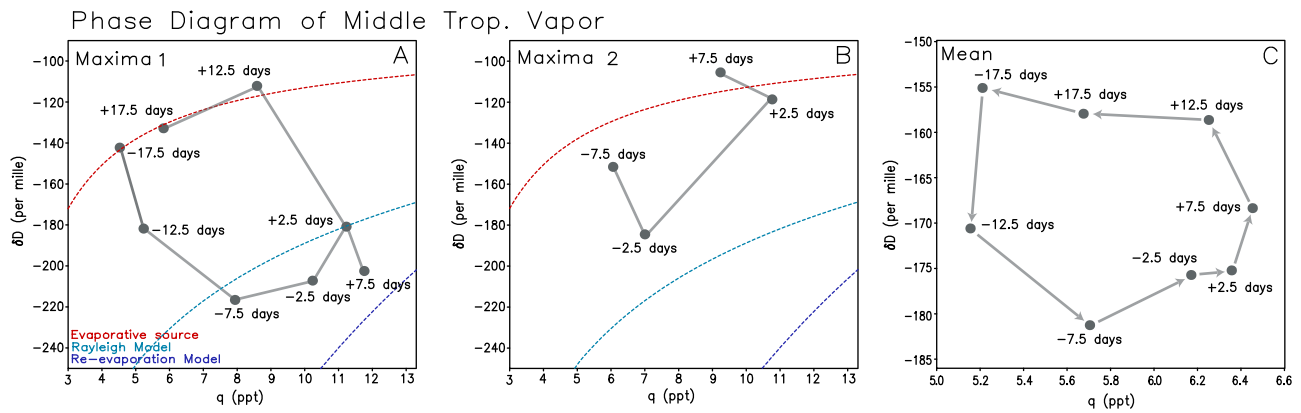


Figure 8. Composite phase diagrams of the joint behavior of H_2O and δD during the passing of an MJO event based on the PDF maps shown in Figure 7. (a) Calculated using the leading extrema of the PDF anomaly maps (see filled contours in Figure 7). (b) As the MJO event develops, a single extrema is replaced by multiple and the second leading extrema for each pentad is expressed. (c) The weighted (by H_2O) mean value of δD and H_2O as an MJO event approaches and passes by the region bounded by 12°S to 12°N latitude and 90° – 120° longitude. The axes units are different for Figure 8c than for Figures 8a and 8b because the overall variability is smaller.

difference between the MJO-domain and the WIO is that because the intraseasonal variability is weaker in the WIO, uncertainty in the phase calculations are larger and the sequence as a consequence is less organized.

4.3. Moisture Sources of MJO Through Joint H_2O – δD Analysis

[37] Composite joint PDF anomalies of water and δD (based on events from Table 1) are shown in Figure 7 alongside theoretical trajectories associated with moisture undergoing Rayleigh distillation (blue curve), a mixing line between evaporation from an oceanic source and a depleted dry end-member (red curve), and moisture that has undergone rainfall evaporation (purple curve). The models are based on those derived by Noone et al. (submitted manuscript, 2012) and here the initial moisture source is assumed to be vapor in equilibrium with the tropical ocean, with a δD value of -80% . Changes in the joint densities of H_2O and δD during different phases of the MJO provide a perspective on the sequence of moist processes associated with the MJO that is independent of the statistical relationships derived from the phase relationships between the isotopic composition of the moisture and selected meteorological fields described in the previous section.

[38] For each MJO phase, the joint PDF for the region based on all available observations (i.e. 2005–2009), is subtracted from the observed with red (blue) indicating the presence of moisture that is in a higher (lower) concentration than the mean state for this region (auxiliary material Figure S2). Approximately 15–20 days prior to the peak in MJO precipitation (Figure 7a), the moisture at the 600–700 hPa level is anomalously composed of moisture that has been directly evaporated from a warm oceanic source. This observation is supported by Figure 5 where the maximum lag between surface evaporation and δD is close to Day 00 and therefore suggests tight phasing between these two fields. As the MJO develops (Figures 7b and 7c), the

evaporative source transitions into one characterized by moisture that has undergone distillation as indicated by its closer proximity to a Rayleigh distillation line. This shift in moisture occurs approximately coincident with the transition from the maximum in evaporative flux to the maximum in easterly moisture convergence as depicted in the phase analysis (Figure 5).

[39] As an MJO event reaches its peak (Figures 7d–7f), the moisture PDFs bifurcate providing evidence for the presence of multiple distinct moisture sources. The presence of moisture that falls well below the Rayleigh distillation line has previously been interpreted to indicate the presence of moisture derived from the evaporation of falling liquid precipitation [Worden et al., 2007]. A second maximum occurs along the trajectory associated with moisture directly originating from evaporation from an oceanic source and a third maximum is associated with an extremely dry air mass, which may be associated with subsiding air. The increasing complexity of the PDFs may, in part, reflect that the inner cloud structure of the MJO is diverse, including both eastward propagating convective clouds and a westward moving cloud shield [Yamada et al., 2010]. The multitude of cloud structures would add complexity through the influence that cloud properties have on isotopic retrievals [e.g., Lee et al., 2011]. With progressive time (Figures 7g and 7h), the air begins to dry out, little moisture is seen near or below the Rayleigh distillation line and the moisture is replaced by an evaporative source comparable to that observed during the initiation stage.

[40] A phase diagram of this sequence is generated using both the composite mean δD and H_2O values (Figure 8c) and by calculating the extrema from each of the PDF anomaly maps (Figures 8a and 8b). The phase maps of the extrema are useful in clearly distinguishing the characteristics of the specific moisture source(s) associated with each phase of the MJO (Figures 8a and 8b), while the phase diagram of the mean PDF anomaly reveals characteristic aspects of

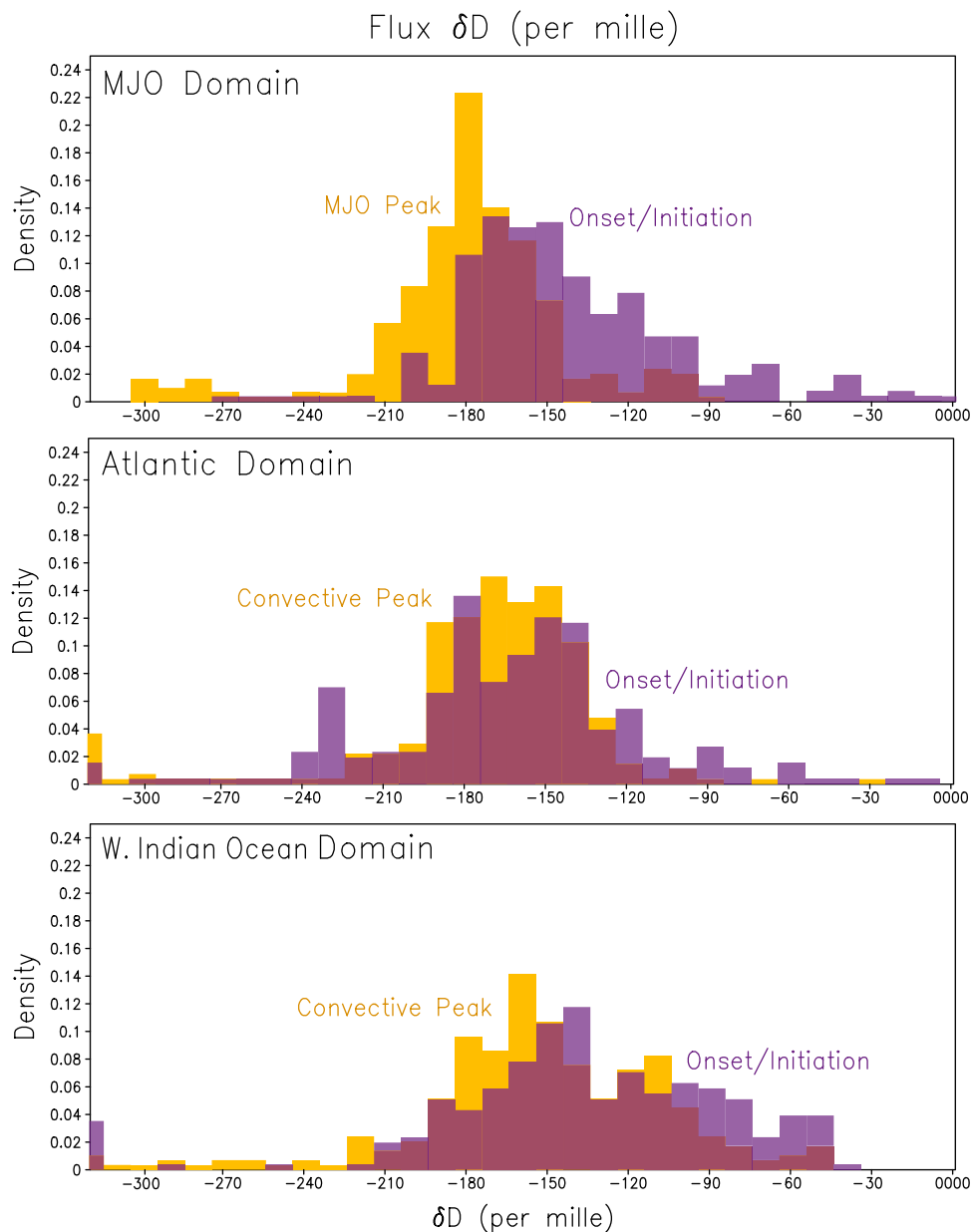


Figure 9. (top) The distribution of the isotopic values for the daily moisture flux during the initiation and peak of MJO events following equations (2) and (3). Moisture fluxes associated with intraseasonal variability in the (middle) N. Atlantic and (bottom) western Indian Ocean are also shown to contrast how moisture flux in the MJO changes during the system’s evolution whereas the values remain nearly stable for the alternative convective systems. Please refer to the text for a description of the budget equation used to calculate the flux values.

the total moisture field. For simplicity, only the leading two extrema are presented and therefore Figures 8a and 8b neglect some of the complexity of Figures 7d–7f.

[41] The phase analysis in Figure 8c suggests that during the initiation stage of the MJO, the moisture transitions from being relatively enriched in the heavy isotope to being progressively depleted as the system develops. The initial isotopic changes occur despite the fact that there were only modest change in total humidity, which results in a downward vertical trajectory in the H_2O – δD space. This marks a transition where the moisture type is shifting with no concomitant change in total moisture. Thus, the rates of moisture

loss and gain are roughly balanced but the source of moisture has changed. Based on the phase analysis between δD and climate fields from Figure 5, the vertical trajectory most likely marks the transition between an evaporative source and one derived from zonal moisture convergence, though the latter is more difficult to constrain. This is further confirmed by the observation that the maximum of the moisture anomaly plots along the theoretical trajectory associated with moisture from an evaporative source but becomes displaced from this trajectory as the system matures.

[42] The isotopic composition of the moisture that brings about the rise in H_2O is estimated using equations (2) and

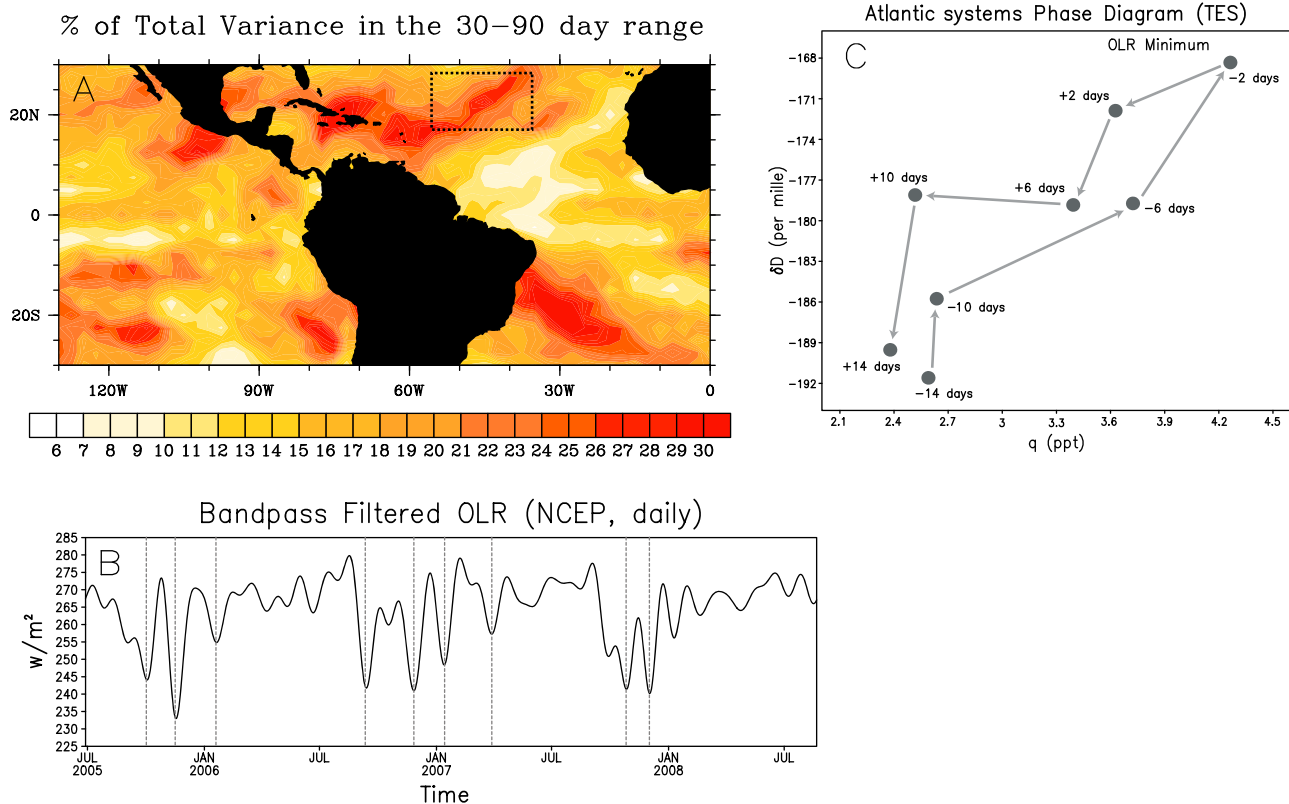


Figure 10. The isotopic phase diagram for a region of the N. Atlantic. (a) The percentage of total OLR variability that is in the 30–90 day window, which was used to identify a region with sustained Convective systems that are somewhat comparable to the MJO. (b) shows an areally averaged time series of OLR that has been filtered to include only variability in the 30–90 day range. The dotted lines highlight the systems that were included in (c) the composite phase diagram. A slightly more compressed time window was used for this Phase diagram than the one shown in Figure 8 to accommodate the shorter longevity of these systems relative to the MJO.

(3). For each day of the moistening, a cumulative δD_{flux} is calculated for the region bounded by 80–120°E and 12°S–12°N for the first and second half (“initiation/onset” and “peak”, respectively) of the MJO (Figure 9). The difference in mean δD_{flux} between the early and latter stages of the MJO is approximately 30‰ though both are characterized by rather wide distributions of daily flux values. The values during the initiation stage reveal the presence of a long tail of relatively enriched values consistent with moistening by an evaporative source. However, the ends of the tail extend well beyond the ratios that would be expected from oceanic evaporation and while the values are similar to what may be expected from sea spray, it is likely they actually arise as an artifact from the simplicity of the budget model. During the period of MJO peak intensity (i.e. 00 lag), the distribution indicates the presence of a number of smaller populations of moisture fluxes, one of which is very depleted ($\sim -300\%$) and a second small population that is enriched ($\sim -100\%$). Similar to the growing moisture source complexity represented by the changes in the joint PDFs (Figure 7) as the MJO evolves, the analysis from Figure 9 also suggests the presence of multiple distinct moisture sources during the peak of the MJO.

[43] Following the peak in MJO precipitation (i.e. Day +2.5), the atmosphere remains moist while the isotope ratios

increase, which manifests as a positive vertical trajectory in the δD – H_2O phase diagram (Figure 8). This period shows the most marked bifurcation in moisture sources, with one source clearly falling along the evaporative line and the second reaching well below the Rayleigh distillation curve. The sequence concludes along a horizontal trajectory in the H_2O – δD space where the air is drying but maintaining a largely stable isotopic value. Mixing between a dry end-member and an air mass that is populated with evaporation (i.e. red curve in Figure 7a) produces a similar effect, because the mixing of dry air would reduce the overall concentration of water in the air but would provide too little moisture to influence the isotopic value. Large-scale subsidence following the peak in MJO activity and the concomitant rise in surface evaporation because of a decrease in cloudiness is consistent with the observed response in the H_2O – δD space.

4.4. A Comparison Between the MJO and Atlantic Convection

[44] In order to test the uniqueness of the MJO phase diagram relative to other sustained convective systems, the analysis described above is replicated for a region in the N. Atlantic that has similar intraseasonal variability but is clearly not directly related to the MJO (Figure 10a). The

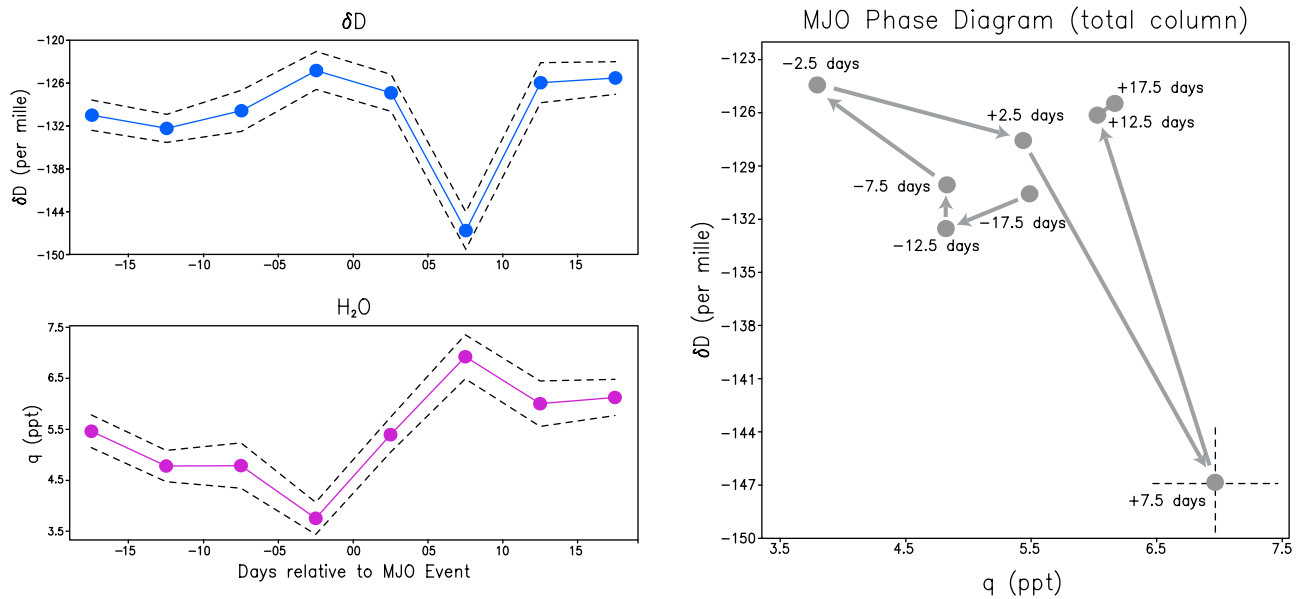


Figure 11. Composite time series’ of boundary layer (bottom left) H_2O and (top left) δD during the passing of an MJO event from the SCIAMACHY data set [Frankenberg *et al.*, 2009]. Uncertainty bounds (dotted) lines are \pm one standard error of the field. (right) The relationship between H_2O and δD over time as the event passes by.

OLR time series for this region reveals a number of sustained organized convective events (Figure 10b), which are used in composite to produce a similar isotopic phase diagram as has been done for the MJO (Figure 8). The timescale of the analysis was reduced to accommodate the shorter longevity of these systems relative to the MJO. The results from this analysis (Figure 10c) indicate the presence of a clearly defined quasi-linear trajectory of H_2O – δD over the life cycle of these convective systems. It is beyond the scope of this study to discuss in detail the significance of this cycle, however its linear nature suggests perhaps only a single predominant moistening source. For example, moistening principally through marine evaporation and then mixing with a dry source (such as easterly winds from Africa) would yield this type of trajectory. The moisture feeding the convection in this region thus appears more uniform than the stepwise moisture source transitions that characterize the life cycle of the MJO.

4.5. Relationship of Boundary Layer and Midtropospheric Moisture

[45] A similar phase diagram for the MJO is also calculated for the boundary layer using HDO retrievals from SCIAMACHY (Figure 11). The data is considerably more uncertain than TES and thus interpretation of small features needs to be treated with additional caution. Boundary layer H_2O appears to show a slow drying during the onset of the MJO and only begins to rise significantly during the peak in MJO precipitation. The boundary layer remains moist in the days following the passage of the event. This disagrees with more robust estimates of atmospheric moisture during the MJO [Tian *et al.*, 2010] and highlights the uncertainty inherent to this data set with respect to analysis over the ocean and at the spatiotemporal resolution of this analysis. The δD field remains reasonably constant in the days leading

up to the peak in MJO activity and then drops 20‰ following the peak of the event. While acknowledging the uncertainty in these estimates, the average δD values are comparable to those observed directly through cryogenic trapping of vapor and direct isotopic measurements by Kurita *et al.* [2012] and the timing and magnitude of the boundary layer minima following the MJO peak also agree with the direct observations. When plotted in H_2O – δD space, the boundary layer air contains an anomalous feature with particularly low δD at high humidity shortly following the MJO peak, suggesting that the boundary layer has been influenced by similar post-condensational exchange processes as observed in the mid-troposphere (Figure 8).

[46] The difference between the mean boundary layer and middle troposphere δD is used to produce an estimate of the “isotopic lapse rate” for the MJO life cycle (Figure 12). The isotopic lapse rate varies in response to changes in precipitation efficiency and vertical mixing such that during periods of high precipitation efficiency there is a steep gradient (with δD depleting as a function of height) as moisture with relatively high isotope ratios is progressively rained out [Ehhalt, 1971; Ehhalt *et al.*, 2005]. On the contrary, when the precipitation efficiency is reduced and high δD boundary layer air is exported vertically and detrained in the mid-troposphere with limited rainout, the result is a more homogeneous profile [Bony *et al.*, 2008]. In addition, the downward mixing of depleted air through downdrafts, precipitation evaporation and ice sublimation can produce a comparable effect [Jouzel, 1986; Risi *et al.*, 2008]. Alternatively, the isotopic lapse rate can reflect disconnectedness between different layers of the atmosphere, where convergence of moisture at one height might produce an isotopic change that is indistinguishable at other levels.

[47] During the initiation stage of the MJO, there is a weak vertical isotopic gradient (Figure 12b), implying that

δD Vapor vertical gradient

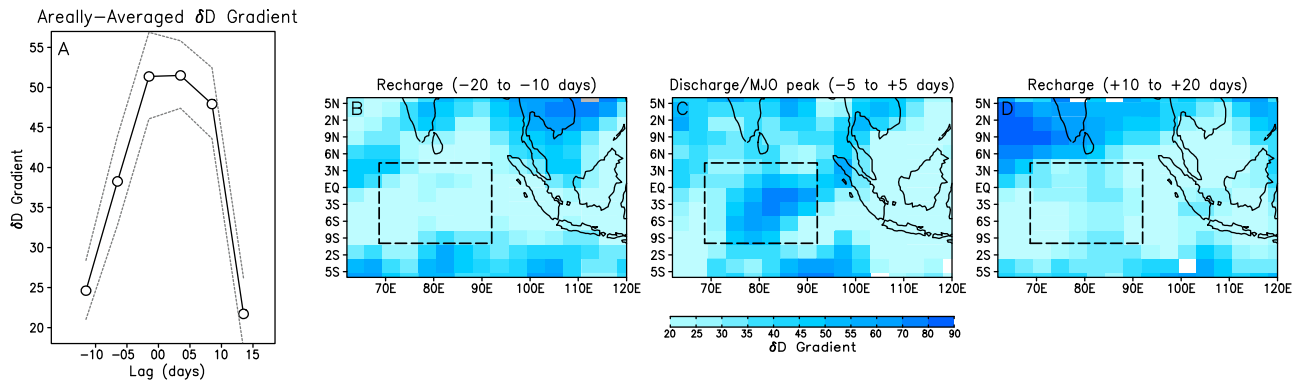


Figure 12. Vertical δD gradient calculated as the difference between the composite δD for SCIAMACHY and TES retrievals during the passing of an MJO event. See text for details on data screening and compositing approach. (a) The mean gradient calculated using the the region inside the dotted square in Figures 12b–12d.

moisture at the TES retrieval level has experienced minimal distillation with respect to the moisture in the boundary layer. This is consistent with the development of a deep boundary layer during the initiation stage, similar to that suggested by *Blade and Hartmann* [1993]. During the buildup phase of the MJO, burn-off from shallow cumulus clouds could produce this effect by transporting boundary layer total water vertically while not producing the depleting affects associated with rainout. There is no fractionation between the water isotopologues of cloud water and atmospheric vapor if the evaporation of cloud condensate is complete. While the shallow gradient, could also reflect vertical homogenization by downward mixing of depleted air, the relatively enriched isotopic values in the mid-troposphere during the onset stage, suggest this is not the likely mechanism. During the development of MJO activity, the gradient reaches a maxima where mid-level moisture is depleted relative to the boundary layer δD by 50‰ (Figure 12c). When the gradient begins to develop (Day -7.5), this is coincident with the maximum in zonal convergence and a lack of any significant isotopic or total water changes in boundary layer moisture (i.e. the change in gradient only reflects mid-tropospheric processes). Convergence of depleted moisture in the mid-troposphere, perhaps associated with Rossby Wave propagation, could produce this result by only minimally influencing the boundary layer isotopic ratios. The gradient continues to develop in-step with a reduction in boundary layer and mid-tropospheric isotopic ratios. The magnitude of the isotopic gradient at the peak of the MJO is consistent with one that would develop during a period of high precipitation efficiency [*Jouzel, 1986*]. The gradient is roughly equivalent to a precipitation efficiency of 0.9, compared to 1.0 for complete Rayleigh distillation [e.g., *Kurita et al., 2012, Figure 8*]. After the peak in MJO activity, the gradient is once again reduced (Figure 12d). The analyses from Figures 5 and 7 would suggest that during the initiation stage, moisture in the mid-troposphere is primarily associated with an evaporative source and therefore the relaxed gradient is indicative of vertical mixing of this moisture. As convection becomes

more active, the isotopic lapse rate increases with a rise in precipitation efficiency and more significant processing of the boundary layer moisture. The subsequent relaxation in isotopic gradient during the dissipation stage may arise from the transition between a convective and stratiform domain. Evaporation from falling hydrometeors has been identified during this period of the MJO using latent heat profiles from TRMM [i.e., *Jiang et al., 2009, Figure 6*] and is an additional process, which would act to oppose the formation of a strong isotopic gradient.

5. Discussion

[48] One of the main sources of disagreements regarding a theory for the MJO involves the relative contributions of evaporated moisture and that derived from convergence in providing a moisture source for MJO convective activity. Unraveling this uncertainty has implications concerning whether wave-CISK [*Lindzen and Nigam, 1987*] or the evaporation-wind feedback (WISHE) [*Emanuel, 1987*] are better theoretical models to apply to the MJO [*Benedict and Randall, 2007; Kirtman and Vernekar, 1993*]. The isotopic composition of atmospheric moisture is well-suited to shed light on this topic. Figure 13 provides a schematic summary of how the moisture source sequence unfolds when viewed with the constraint on the water balance offered by the isotopic ratios. During the early initiation stage of the MJO (15–20 days prior to the MJO peak), there is strong evidence from the isotope ratios, that the moisture in the lower and mid troposphere is primarily derived from an evaporative source. This is clearly seen in Figures 7 and 8, by the presence of a positive moisture anomaly that falls along the trajectory associated with mixing between an evaporative moisture source and dry air. In the onset stage of the MJO, there is a very weak gradient in isotopic ratios between the boundary layer and 600–700 hPa level (Figure 12), indicating that the evaporative source is being mixed vertically with little depletion associated with rainout. This observation would support the argument that evaporation is the predominant moisture source responsible for boundary-layer

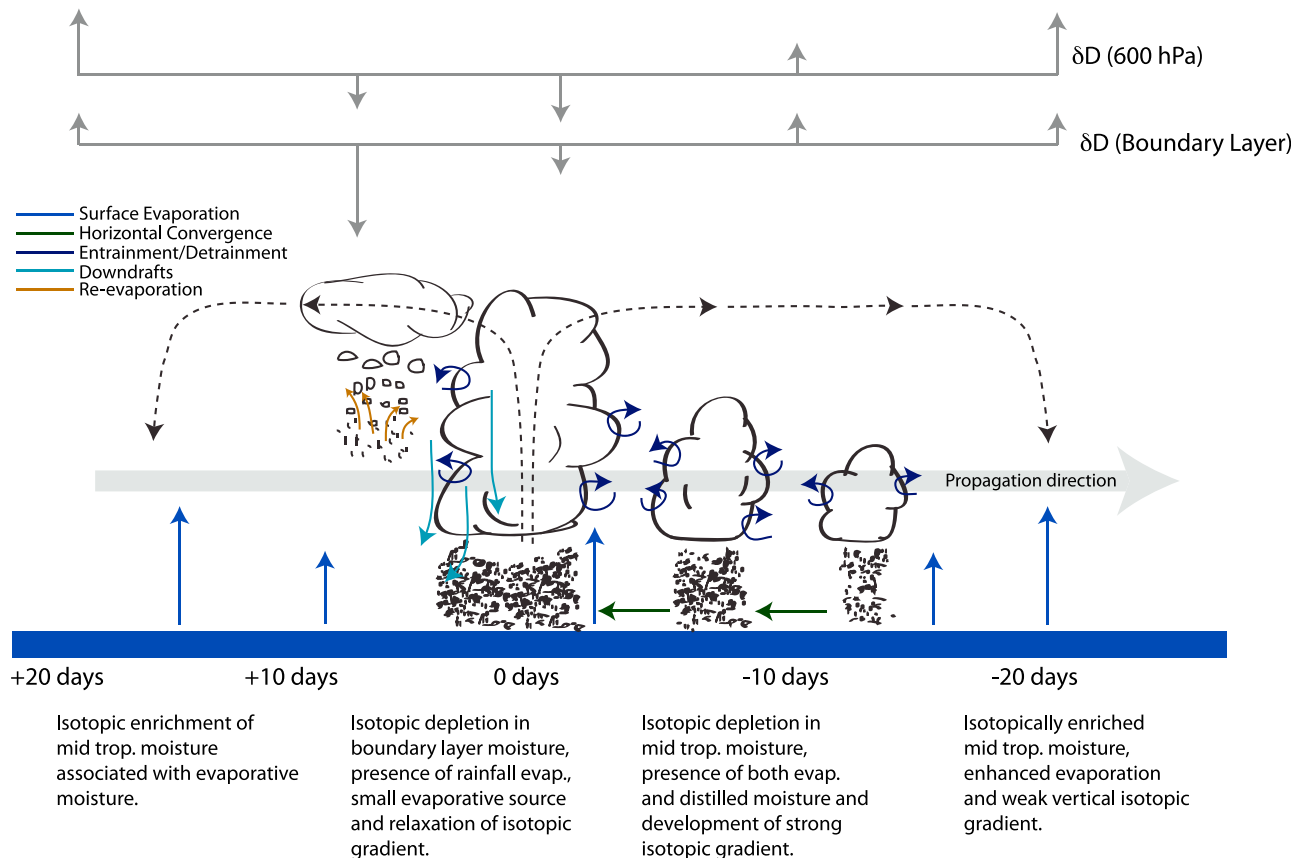


Figure 13. Schematic diagram showing basic isotopic and meteorological aspects of a propagating MJO event. Blue arrows indicate evaporative flux from the ocean, green arrows represent flux from easterly convergence, purple arrows are detrainment from clouds, light blue represent unsaturated downdrafts and orange are fluxes from evaporation/exchange of hydrometeors. The arrow lengths qualitatively correspond to the magnitude of the flux.

pre-conditioning of the MJO [Araligidad and Maloney, 2008; Maloney and Sobel, 2004].

[49] During the following pentad (10–15 days), the moisture falls below that typical of a purely evaporative source [Worden *et al.*, 2007]. This change occurs synchronous with the rise in zonal moisture convergence, which both Benedict and Randall [2007] and Waliser *et al.* [2009] argue to be the major source of MJO moisture. The signature of evaporated moisture in the earlier pentads is quite clear from the joint H_2O – δD analysis however, it is considerably more challenging to clearly delineate moisture sourced from convergence. The isotope ratio of this moisture source would vary based on its history and origin [Brown *et al.*, 2008] and therefore without extensive trajectory analysis, its presence is argued here on the basis of the increase of convergence at this period in the sequence. Furthermore, Figure 2 suggests that Rossby waves and mean easterly flow may propagate a depleted isotopic source downstream and could thus produce this depletion of the mid-tropospheric atmospheric moisture. The transition in isotope ratios at this period of the MJO is thus interpreted to predominantly mark a change from an evaporative to a convergent source, consistent with the findings of Weare [2003] and Kirtman and Vernekar [1993]. This favors a WISHE-CISK switch during the build-up of

MJO events. In the isotope-phase diagram (Figure 8) this transition manifests as a downward vertical trajectory in the δD – H_2O space. Because the isotopic change occurs amidst a background of relatively constant total moisture content, previous observations of the moisture dynamics of the MJO based on specific humidity alone [e.g., Tian *et al.*, 2010; Myers and Waliser, 2003] are not able to identify this transition.

[50] The moisture source sequence derived with insight from the water vapor isotope ratios does differ in some ways from Weare [2003] and Kirtman and Vernekar [1993], in that the moisture anomaly maps become increasingly complex as the peak of convection approaches. While some of this complexity may arise as a product of the satellite's sensitivity to the diversity of the MJO's inner cloud structure, the consistency between the moisture sources implied from the joint-PDF analysis (Figures 7 and 8) and theoretical models of H_2O – δD trajectories undergoing mixing and rainout, support the interpretation of the data as being largely a product of changes in moisture sources as opposed to satellite sensitivity. Five to ten days before the MJO maximum, there is evidence of a bimodal distribution in the PDF anomaly maps (Figures 7, 8 and 9) suggesting both a positive evaporative anomaly as well as moisture associated with

a more depleted source. As discussed by *Thayer-Calder and Randall* [2009], positive feedbacks between precipitation rate and surface wind speed lead to both enhanced evaporation and moisture convergence anomalies as the peak of the MJO approaches. Therefore, as the system matures, these two distinct moisture sources become apparent. This observation is in contrast to *Weare* [2003], who suggests there is a singularly well-defined transition between dominant sources during the early stages of the MJO. *Thayer-Calder and Randall* [2009] argue based on results from a super-parametrized climate model simulation, that both evaporative and convergent moisture sources are theoretically required to maintain sufficient moisture in the atmosphere to inhibit downdrafts, which would stabilize the column against convection. Although stabilization is not an aspect quantified here, we do provide evidence for these two distinct water sources in support of their conjecture.

[51] In the days just after the peak in MJO activity, the $\text{H}_2\text{O}-\delta\text{D}$ PDFs (Figures 7 and 8) depict an increasing presence of moisture falling well below the Rayleigh distillation line. This occurs in step with a rise in stratiform cloud cover (Figure 5), a sharp drop in the boundary layer δD (Figure 11) and a relaxation of the vertical δD gradient (Figure 12). These observations suggest that evaporation from falling liquid hydrometeors are a critical component of the MJO atmosphere during and immediately following the peak in convective activity. *Jiang et al.* [2009] also document the presence of a similar feature based on latent heating profiles of the MJO. Convective systems in the western Indian Ocean, which tend to be shorter lived than those in the MJO domain, do not show a significant phase relationship with rainfall evaporation (Figure 5). Because rainfall evaporation is tied to stratiform rainfall, the absence of this moisture in the western Indian Ocean and its presence in the MJO domain lends support to the notion that stratiform heating is necessary for MJO sustenance [*Lin et al.*, 2004; *Kurita et al.*, 2012].

[52] The isotopic diagnoses ultimately depict multiple transitions associated with the moisture source sequence for the MJO. The extent to which this specific sequence is in fact necessary for the MJO to develop or simply a byproduct of other processes is a question best suited for a modeling study where the hypothesized moisture sources could be prescribed and the impact on the MJO directly assessed. A series of preliminary attempts to address this however are done here by comparing the moisture source sequence for the MJO and for convective systems in both the Western Indian Ocean and subtropical North Atlantic. As shown in Figure 9, both non-MJO systems lack a significant shift in the isotopic composition of the moisture flux during their respective onset and peak convective periods. This suggests these systems are more reliant on moistening from a single source and lack the multistage sequence of sources of the MJO. This is also exhibited in the phase diagram for the Atlantic systems (Figure 10c), where the atmosphere moistens and dehydrates along a nearly linear trajectory. It has been argued that the failures of GCMs to produce MJO-like systems is because of an inability to resolve the dynamical processes that lead to convective self-suppression where the atmosphere moistens and rains out without developing moisture-convection feedbacks. It thus may be that the difference between the linear $\text{H}_2\text{O}-\delta\text{D}$ trajectory in

the Atlantic systems and the phase-“wheel” for the MJO embodies one aspect of why GCMs are unable to consistently yield MJO-like structures.

6. Conclusions

[53] It is clear from the analyses of the TES HDO and H_2O retrievals, that the MJO produces a strong influence on the δD of mid-tropospheric atmospheric humidity. The signal is distinct from the H_2O field alone and therefore provides novel information on moisture dynamics associated with MJO development. The strength of the signal is arguably as well-pronounced as that derived from OLR, which is considered the benchmark field by which to observe the MJO. Fundamentally, this indicates that the life cycle of the MJO involves sequential changes in its moisture source and tropospheric hydrology. Although the results have been focused primarily on the MJO, the space-time spectra and Hovmöller plot of δD highlight other salient features of tropical isotopic hydrology including a strong signal associated with Rossby waves and an absence of a signature associated with Kelvin waves. The Rossby wave signature is strongest in the eastern Tropical Pacific (Figure 2) and, unlike the MJO, is not associated with organized convection. It is likely that this signal reflects changes in horizontal advection and variations in the strength of Walker circulation but validation of this assertion would require additional analyses, which extend beyond the scope of this paper. The shared absence of a Kelvin wave signature in both latent heat flux and δD fields, suggests a certain global sensitivity of the isotopic composition of moisture to surface moisture flux and as well may reflect the fact that Kelvin waves are not associated with material transport and therefore do not maintain information on moisture histories.

[54] Analysis of the isotopic composition of atmospheric water vapor over the MJO-domain provides clarification on a standing debate surrounding the source of moisture that feeds the MJO. The isotopic analysis provides robust evidence that evaporative moisture occupies the mid-troposphere in the early onset period of the system. While the prevalence of this source disappears during early convective development, it re-emerges during the peak of MJO activity. The multisource sequence for the MJO presented here is broadly consistent with results from super-parametrized GCM simulations that produce MJO-like features though the isotopic information better resolves the complex interplay between components identified elsewhere.

[55] The isotopic changes in the atmospheric column lead the maxima in convective activity by multiple weeks. Therefore real-time monitoring of water vapor isotope ratios over the Indian Ocean could potentially prove beneficial in MJO forecasting if it could be shown that the preconditioning of the atmospheric boundary layer is truly requisite for MJO formation. If the well-defined transitions in the phase diagrams (Figure 8) could be used to objectively delineate whether a convective system was going to dissipate in isolation or become sustained following the multisource MJO sequence, than isotope ratio data could be used in conjunction with other forecasting tools to improve forecasting skill. Follow-up studies using in situ isotopic measurements with altitudinal cross-sections done in conjunction with high-resolution measurements of the isotopic composition of

precipitation (a sink term) would certainly be necessary before isotopes could be actively employed as an index to aid in identifying the onset of an MJO. In addition, as cloud-resolving-models [Grabowski, 2003; Miura et al., 2007] and models with super parameterization schemes [Randall et al., 2003; Thayer-Calder and Randall, 2009] continue to develop more realistic MJO events, the inclusion of isotope tracers in these simulations would provide a useful diagnostic to compare the realism of different simulations, particularly with respect to the correct representation of the hydrological processes that accompany the build-up phase of the system. The results presented here thus serve as a benchmark to assess the extent to which simulated MJOs are being produced by the appropriate dynamical processes.

[56] **Acknowledgments.** The authors would like to thank John Worden and Derek Brown for assistance in processing the TES data. Christian Frankenberg and Remco Sheepmaker for sharing the SCHIAMACHY data. George Kiladis, Matthew Wheeler, Dennis Shea and Daehyun Kim for sharing useful codes for MJO diagnostic analysis. The work was supported by grants from the NASA Atmospheric Composition Program (NNX08AR23G) and the NASA Energy and Water Cycle Study (07-NEWS07-0020).

References

- Adler, R., et al. (2003), The Version-2 Global Precipitation Climatology Project(GPCP) monthly precipitation analysis(1979-present), *J. Hydro-meteorol.*, *4*(6), 1147–1167.
- Agudelo, P., J. Curry, C. Hoyos, and P. Webster (2006), Transition between suppressed and active phases of intraseasonal oscillations in the Indo-Pacific warm pool, *J. Clim.*, *19*(21), 5519–5530.
- Araligidad, N., and E. Maloney (2008), Wind-driven latent heat flux and the intraseasonal oscillation, *Geophys. Res. Lett.*, *35*, L04815, doi:10.1029/2007GL032746.
- Benedict, J., and D. Randall (2007), Observed characteristics of the MJO relative to maximum rainfall, *J. Atmos. Sci.*, *64*(7), 2332–2354.
- Bigeleisen, J. (1961), Statistical mechanics of isotope effects on the thermodynamic properties of condensed systems, *J. Chem. Phys.*, *34*, 1485, doi:10.1063/1.1701033.
- Blade, I., and D. Hartmann (1993), Tropical intraseasonal oscillations in a simple nonlinear model, *J. Atmos. Sci.*, *50*(17), 2922–2939.
- Bony, S., C. Risi, and F. Vimeux (2008), Influence of convective processes on the isotopic composition ($\delta^{18}\text{O}$ and δD) of precipitation and water vapor in the tropics: 1. Radiative-convective equilibrium and Tropical Ocean-Global Atmosphere-Coupled Ocean-atmosphere Response Experiment (TOGA-COARE) simulations, *J. Geophys. Res.*, *113*, D19305, doi:10.1029/2008JD009942.
- Botev, Z., J. Grotowski, and D. Kroese (2010), Kernel density estimation via diffusion, *Ann. Stat.*, *38*(5), 2916–2957.
- Brown, D., J. Worden, and D. Noone (2008), Comparison of atmospheric hydrology over convective continental regions using water vapor isotope measurements from space, *J. Geophys. Res.*, *113*, D15124, doi:10.1029/2007JD009676.
- Camargo, S., M. Wheeler, and A. Sobel (2009), Diagnosis of the MJO modulation of tropical cyclogenesis using an empirical index, *J. Atmos. Sci.*, *66*(10), 3061–3074, doi:10.1175/2009JAS3101.1.
- Cassou, C. (2008), Intraseasonal interaction between the Madden-Julian Oscillation and the North Atlantic Oscillation, *Nature*, *455*(7212), 523–527, doi:10.1038/nature07286.
- Chave, A., D. Thomson, and M. Ander (1987), On the robust estimation of power spectra, coherences, and transfer functions, *J. Geophys. Res.*, *92*(B1), 633–648, doi:10.1029/JB092iB01p00633.
- Craig, H., and L. Gordon (1965), Deuterium and ^{18}O variations in the ocean and the marine atmosphere, in *Proceedings of a Conference on Stable Isotopes in Oceanographic Studies and Paleotemperatures*, vol. 3, edited by E. Tongiorgi, pp. 9–130, CNR, Spoleto, Italy.
- Dansgaard, W. (1964), Stable isotopes in precipitation, *Tellus*, *16*, 436–468.
- Ehhalt, D. (1971), Vertical profiles and transport of HTO in the troposphere, *J. Geophys. Res.*, *76*(30), 7351–7367, doi:10.1029/JC076i030p07351.
- Ehhalt, D., F. Rohrer, and A. Fried (2005), Vertical profiles of HDO/H₂O in the troposphere, *J. Geophys. Res.*, *110*, D13301, doi:10.1029/2004JD005569.
- Emanuel, K. (1987), An air-sea interaction model of intraseasonal oscillations in the tropics, *J. Atmos. Sci.*, *44*(16), 2324–2340.
- Emanuel, K. (1989), The finite-amplitude nature of tropical cyclogenesis, *J. Atmos. Sci.*, *46*(22), 3431–3456.
- Frankenberg, C., et al. (2009), Dynamic processes governing lower-tropospheric HDO/H₂O ratios as observed from space and ground, *Science*, *325*(5946), 1374–1377, doi:10.1126/science.1173791.
- Friedman, I., A. Redfield, B. Schoen, and J. Harris (1964), The variation of the deuterium content of natural waters in the hydrologic cycle, *Rev. Geophys.*, *2*(1), 177–224, doi:10.1029/RG002i001p00177.
- Galewsky, J., M. Strong, and Z. Sharp (2007), Measurements of water vapor D/H ratios from Mauna Kea, Hawaii, and implications for subtropical humidity dynamics, *Geophys. Res. Lett.*, *34*, L22808, doi:10.1029/2007GL031330.
- Gat, J. R. (2000), Atmospheric water balance—The isotopic perspective, *Hydrol. Processes*, *14*(8), 1357–1369.
- Grabowski, W. (2003), MJO-like coherent structures: Sensitivity simulations using the cloud-resolving convection parameterization (CRCP), *J. Atmos. Sci.*, *60*(6), 847–864.
- Grabowski, W., and M. Moncrieff (2004), Moisture-convective feedback in the tropics, *Q. J. R. Meteorol. Soc.*, *130*(604), 3081–3104.
- Hendon, H., and M. Salby (1994), The life cycle of the Madden-Julian Oscillation, *J. Atmos. Sci.*, *51*(15), 2225–2237.
- Hendon, H., B. Liebmann, and J. Glick (1998), Oceanic Kelvin waves and the Madden-Julian Oscillation, *J. Atmos. Sci.*, *55*(1), 88–101.
- Jiang, X., et al. (2009), Vertical heating structures associated with the MJO as characterized by TRMM estimates, ECMWF reanalyses, and forecasts: A case study during 1998/99 winter, *J. Clim.*, *22*(22), 6001–6020, doi:10.1175/2009JCLI3048.1.
- Johnson, R., T. Rickenbach, S. Rutledge, P. Ciesielski, and W. Schubert (1999), Trimodal characteristics of tropical convection, *J. Clim.*, *12*(8), 2397–2418.
- Jones, C., and B. Weare (1996), The role of low-level moisture convergence and ocean latent heat fluxes in the Madden and Julian Oscillation: An observational analysis using ISCCP data and ECMWF analyses, *J. Clim.*, *9*(12), 3086–3104.
- Joussaume, S., R. Sadourmy, and J. Jouzel (1984), A general-circulation model of water isotope cycles in the atmosphere, *Nature*, *311*(5981), 24–29.
- Jouzel, J. (1986), Isotopes in cloud physics: Multiphase and multistage condensation processes, in *Handbook of Environmental Isotope Geochemistry*, vol. 2, pp. 61–112, Elsevier, New York.
- Kanamitsu, M., et al. (2002), NCEP dynamical seasonal forecast system 2000, *Bull. Am. Meteorol. Soc.*, *83*(7), 1019–1038.
- Kemball-Cook, S., and B. Weare (2001), The onset of convection in the Madden-Julian Oscillation, *J. Clim.*, *14*(5), 780–793.
- Kiladis, G., K. Straub, and P. Haertel (2005), Zonal and vertical structure of the Madden-Julian Oscillation, *J. Atmos. Sci.*, *62*(8), 2790–2809.
- Kiladis, G., M. Wheeler, P. Haertel, K. Straub, and P. Roundy (2009), Convectively coupled equatorial waves, *Rev. Geophys.*, *47*, RG2003, doi:10.1029/2008RG000266.
- Kim, D., et al. (2009), Application of MJO simulation diagnostics to climate models, *J. Clim.*, *22*(23), 6413–6436.
- Kirtman, B., and A. Vernekar (1993), On wave-CISK and the evaporation-wind feedback for the Madden-Julian Oscillation, *J. Atmos. Sci.*, *50*, 2811–2816.
- Kurita, N., K. Ichianagi, J. Matsumoto, M. Yamanaka, and T. Ohata (2009), The relationship between the isotopic content of precipitation and the precipitation amount in tropical regions, *J. Geochem. Explor.*, *102*(3), 113–122.
- Kurita, N., D. Noone, C. Risi, G. Schmidt, H. Yamada, and K. Yoneyama (2011), Intraseasonal isotopic variation associated with the Madden-Julian Oscillation, *J. Geophys. Res.*, *116*, D24101, doi:10.1029/2010JD015209.
- Lawrence, J. R., S. D. Gedzelman, D. Dexheimer, H. K. Cho, G. D. Carrie, R. Gasparini, C. R. Anderson, K. P. Bowman, and M. I. Biggerstaff (2004), Stable isotopic composition of water vapor in the tropics, *J. Geophys. Res.*, *109*, D06115, doi:10.1029/2003JD004046.
- Lee, J., J. Worden, D. Noone, K. Bowman, A. Eldering, A. LeGrande, J. Li, G. Schmidt, and H. Sodemann (2011), Relating tropical ocean clouds to moist processes using water vapor isotope measurements, *Atmos. Chem. Phys. Discuss.*, *11*, 741–752.
- Lee, J. E., and I. Fung (2008), “Amount effect” of water isotopes and quantitative analysis of post-condensation processes, *Hydrol. Processes*, *22*(1), 1–8.
- Lee, J. H., X. H. Feng, E. S. Posmentier, A. M. Faiia, and S. Taylor (2009), Stable isotopic exchange rate constant between snow and liquid water, *Chem. Geol.*, *260*(1–2), 57–62.
- Lee, M. I., I. S. Kang, and B. E. Mapes (2003), Impacts of cumulus convection parameterization on aqua-planet AGCM simulations of tropical intraseasonal variability, *J. Meteorol. Soc. Jpn.*, *81*(5), 963–992.

- Li, K., B. Tian, D. Waliser, and Y. Yung (2010), Tropical mid-tropospheric CO₂ variability driven by the Madden-Julian Oscillation, *Proc. Natl. Acad. Sci. U. S. A.*, *107*(45), 19,171–19,175.
- Liebmann, B., and C. Smith (1996), Description of a complete (interpolated) outgoing longwave radiation dataset, *Bull. Am. Meteorol. Soc.*, *77*(6), 1275–1277.
- Lin, J., B. Mapes, M. Zhang, and M. Newman (2004), Stratiform precipitation, vertical heating profiles, and the Madden-Julian Oscillation, *J. Atmos. Sci.*, *61*(3), 296–309.
- Lindzen, R., and S. Nigam (1987), On the role of sea surface temperature gradients in forcing low-level winds and convergence in the tropics, *J. Atmos. Sci.*, *44*(17), 2418–2436.
- Madden, R., and P. Julian (1971), Detection of a 40–50 day oscillation in the zonal wind in the tropical Pacific, *J. Atmos. Sci.*, *28*(5), 702–708.
- Madden, R., and P. Julian (1972), Description of global-scale circulation cells in the tropics with a 40–50 day period, *J. Atmos. Sci.*, *29*, 1109–1123.
- Majda, A., and S. Stechmann (2009), The skeleton of tropical intraseasonal oscillations, *Proc. Natl. Acad. Sci. U. S. A.*, *106*(21), 8417–8422.
- Majda, A., S. Stechmann, and B. Khouider (2007), Madden-Julian Oscillation analog and intraseasonal variability in a multcloud model above the equator, *Proc. Natl. Acad. Sci. U. S. A.*, *104*(24), 9919–9924.
- Majoube, M. (1971), Oxygen-18 and deuterium fractionation between water and steam, *J. Chim. Phys. Phys. Chim. Biol.*, *68*(10), 1423–1436.
- Maloney, E., and D. Hartmann (1998), Frictional moisture convergence in a composite life cycle of the Madden-Julian Oscillation, *J. Clim.*, *11*(9), 2387–2403.
- Maloney, E., and A. Sobel (2004), Surface fluxes and ocean coupling in the tropical intraseasonal oscillation, *J. Clim.*, *17*(22), 4368–4386.
- Masunaga, H., T. L'Ecuyer, and C. Kummerow (2006), The Madden-Julian Oscillation recorded in early observations from the Tropical Rainfall Measuring Mission (TRMM), *J. Atmos. Sci.*, *63*(11), 2777–2794.
- Matsuno, T. (1966), Quasi-geostrophic motions in the equatorial area, *J. Meteorol. Soc. Jpn.*, *44*(1), 25–42.
- Matthews, A. (2000), Propagation mechanisms for the Madden-Julian Oscillation, *Q. J. R. Meteorol. Soc.*, *126*(569), 2637–2651.
- Merlivat, L., and J. Jouzel (1979), Global climatic interpretation of the deuterium-oxygen-18 relationship for precipitation, *J. Geophys. Res.*, *84*(C8), 5029–5033.
- Miura, H., M. Satoh, T. Nasuno, A. Noda, and K. Oouchi (2007), A Madden-Julian Oscillation event realistically simulated by a global cloud-resolving model, *Science*, *318*(5857), 1763–1765.
- MJO Clivar Working Group (2009), MJO simulation diagnostics, *J. Clim.*, *22*(11), 3006–3030.
- Myers, D., and D. Waliser (2003), Three-dimensional water vapor and cloud variations associated with the Madden-Julian Oscillation during Northern Hemisphere winter, *J. Clim.*, *16*(6), 929–950.
- Nakazawa, T. (1988), Tropical super clusters within intraseasonal variations over the western Pacific, *J. Meteorol. Soc. Jpn.*, *66*(6), 823–839.
- Noone, D. (2012), Pairing measurements of the water vapor isotope ratio with humidity to deduce atmospheric moistening and dehydration in the tropical mid troposphere, *J. Clim.*, in press.
- Randall, D., M. Khairoutdinov, A. Arakawa, and W. Grabowski (2003), Breaking the cloud parameterization deadlock, *Bull. Am. Meteorol. Soc.*, *84*(11), 1547–1564.
- Ray, P., C. Zhang, J. Dudhia, and S. Chen (2009), A numerical case study on the initiation of the Madden-Julian Oscillation, *J. Atmos. Sci.*, *66*(2), 310–331.
- Raymond, D. (2001), A new model of the Madden-Julian Oscillation, *J. Atmos. Sci.*, *58*(18), 2807–2819.
- Rienecker, M., et al. (2011), MERRA-NASA's modern-era retrospective analysis for research and applications, *J. Clim.*, *24*(14), 3624–3648, doi:10.1175/JCLI-D-11-00015.1.
- Risi, C., S. Bony, and F. Vimeux (2008), Influence of convective processes on the isotopic composition ($\delta^{18}\text{O}$ and δD) of precipitation and water vapor in the tropics: 2. Physical interpretation of the amount effect, *J. Geophys. Res.*, *113*, D19306, doi:10.1029/2008JD009943.
- Risi, C., S. Bony, F. Vimeux, and J. Jouzel (2010), Water-stable isotopes in the LMDZ4 general circulation model: Model evaluation for present-day and past climates and applications to climatic interpretations of tropical isotopic records, *J. Geophys. Res.*, *115*, D12118, doi:10.1029/2009JD013255.
- Rozanski, K., and C. Sonntag (1982), Vertical distribution of deuterium in atmospheric water vapour, *Tellus*, *34*(1), 135–141.
- Seo, K., and K. Kim (2003), Propagation and initiation mechanisms of the Madden-Julian Oscillation, *J. Geophys. Res.*, *108*(D13), 4384, doi:10.1029/2002JD002876.
- Singh, S., R. Kripalani, and D. Sikka (1992), Interannual variability of the Madden-Julian Oscillations in Indian summer monsoon rainfall, *J. Clim.*, *5*, 973–979.
- Slingo, J., et al. (1996), Intraseasonal oscillations in 15 atmospheric general circulation models: Results from an AMIP diagnostic subproject, *Clim. Dyn.*, *12*(5), 325–357.
- Sobel, A., E. Maloney, G. Bellon, and D. Frierson (2008), The role of surface heat fluxes in tropical intraseasonal oscillations, *Nat. Geosci.*, *1*(10), 653–657.
- Stewart, M. K. (1975), Stable isotope fractionation due to evaporation and isotopic-exchange of falling waterdrops—Applications to atmospheric processes and evaporation of lakes, *J. Geophys. Res.*, *80*(9), 1133–1146.
- Straub, K., G. Kiladis, and P. Ciesielski (2006), The role of equatorial waves in the onset of the South China Sea summer monsoon and the demise of El Niño during 1998, *Dyn. Atmos. Oceans*, *42*(1–4), 216–238.
- Thayer-Calder, K., and D. Randall (2009), The role of convective moistening in the Madden-Julian Oscillation, *J. Atmos. Sci.*, *66*(11), 3297–3312.
- Tian, B., D. Waliser, E. Fetzer, B. Lambrigtsen, Y. Yung, and B. Wang (2006), Vertical moist thermodynamic structure and spatial-temporal evolution of the Madden-Julian Oscillation in Atmospheric Infrared Sounder observations, *J. Atmos. Sci.*, *63*, 2462–2485.
- Tian, B., D. Waliser, E. Fetzer, and Y. Yung (2010), Vertical moist thermodynamic structure of the Madden-Julian Oscillation in Atmospheric Infrared Sounder retrievals: An update and a comparison to ECMWF Interim Re-Analysis, *Mon. Weather Rev.*, *138*, 4576–4582.
- Tokioka, T., K. Yamazaki, A. Kitoh, and T. Ose (1988), The equatorial 30–60 day oscillation and the Arakawa-Schubert penetrative cumulus parameterization, *J. Meteorol. Soc. Jpn.*, *66*(6), 883–901.
- Uppala, S., et al. (2005), The ERA-40 re-analysis, *Q. J. R. Meteorol. Soc.*, *131*(612), 2961–3012.
- Waliser, D., K. Lau, and J. Kim (1999), The influence of coupled sea surface temperatures on the Madden-Julian Oscillation: A model perturbation experiment, *J. Atmos. Sci.*, *56*(3), 333–358.
- Waliser, D., R. Murtugudde, P. Strutton, and J. Li (2005), Subseasonal organization of ocean chlorophyll: Prospects for prediction based on the Madden-Julian Oscillation, *Geophys. Res. Lett.*, *32*, L23602, doi:10.1029/2005GL024300.
- Waliser, D., B. Tian, X. Xie, W. Liu, M. Schwartz, and E. Fetzer (2009), How well can satellite data characterize the water cycle of the Madden-Julian Oscillation?, *Geophys. Res. Lett.*, *36*, L21803, doi:10.1029/2009GL040005.
- Weare, B. (2003), Composite singular value decomposition analysis of moisture variations associated with the Madden-Julian Oscillation, *J. Clim.*, *16*(22), 3779–3792.
- Webster, C., and A. Heysmsfield (2003), Water isotope ratios D/H, $^{18}\text{O}/^{16}\text{O}$, $^{17}\text{O}/^{16}\text{O}$ in and out of clouds map dehydration pathways, *Science*, *302*, 1742–1746.
- Wheeler, M., and H. Hendon (2004), An all-season real-time multivariate MJO index: Development of an index for monitoring and prediction, *Mon. Weather Rev.*, *132*(8), 1917–1932.
- Wheeler, M., and G. Kiladis (1999), Convectively coupled equatorial waves: Analysis of clouds and temperature in the wavenumber-frequency domain, *J. Atmos. Sci.*, *56*, 374–399.
- Worden, J., et al. (2006), Tropospheric Emission Spectrometer observations of the tropospheric HDO/H₂O ratio: Estimation approach and characterization, *J. Geophys. Res.*, *111*, D16309, doi:10.1029/2005JD006606.
- Worden, J., D. Noone, K. Bowman, and T. E. Spect (2007), Importance of rain evaporation and continental convection in the tropical water cycle, *Nature*, *445*(7127), 528–532.
- Worden, J., D. Noone, J. Galewsky, A. Bailey, K. Bowman, D. Brown, J. Hurlley, S. Kulawik, J. Lee, and M. Strong (2010), Estimate of bias in Aura TES HDO/H₂O profiles from comparison of TES and in situ HDO/H₂O measurements at the Mauna Loa observatory, *Atmos. Chem. Phys. Discuss.*, *11*, 4491–4503.
- Yamada, H., K. Yoneyama, M. Katsumata, and R. Shirooka (2010), Observations of a super cloud cluster accompanied by synoptic-scale eastward-propagating precipitating systems over the Indian Ocean, *J. Atmos. Sci.*, *67*(5), 1456–1473.
- Zhang, C. (2005), Madden-Julian Oscillation, *Rev. Geophys.*, *43*, RG2003, doi:10.1029/2004RG000158.

M. Berkelhammer, D. C. Noone, and C. Risi, Cooperative Institute for Research in Environmental Sciences, University of Colorado at Boulder, Boulder, CO 80309, USA. (max.berkelhammer@colorado.edu)

N. Kurita, Japan Agency for Marine-Earth Science and Technology, 2-15 Natsushimacho, Yokosuka, Japan.